Modeling Pedestrian Tactical and Operational Decisions Under Risk and Uncertainty A Two-Layer Model Framework

Huang, Rong; Zhao, Xuan; Yuan, Yufei; Yu, Qiang; Liu, Chengqing; Daamen, Winnie

DOI
10.1109/TITS.2023.3237335

Publication date
2023

Document Version
Final published version

Published in
IEEE Transactions on Intelligent Transportation Systems

Modeling Pedestrian Tactical and Operational Decisions Under Risk and Uncertainty: A Two-Layer Model Framework

Rong Huang, Xuan Zhao, Yufei Yuan, Qiang Yu, Chengqing Liu, and Winnie Daamen

***Abstract*— Pedestrian tactical choices and operational movement in evacuations essentially pertain to decision-making under risk and uncertainty. However, in microscopic evacuation models, this attribute has been greatly overlooked, even lacking a methodology to delineate the related decision characteristics (bounded rationality and risk attitudes), let alone their effects on evacuation processes. This work presents an innovative two-layer floor field cellular automaton model framework, where three intertwined sub-modules respectively dedicated to modelling the exit choice, the locomotion movement and the exit-choice changing behaviours are proposed and integrated as an entity. By introducing various decision-making elements computed by the proposed algorithm, Cumulative Prospect Theory (CPT) is proposed for the first time to model the exit choice and locomotion decision-making under risk and uncertainty. In the exit-choice changing module, attractive and repulsive forces are invented to jointly describe the tendency to revisit the routing decision. Each sub-module and the whole framework are validated in manifold indoor environments. The simulation results of the modules with CPT accord with the empirics from the evacuation experiments and are superior over those from the state-of-the-art models. The degree of rationality and risk attitudes are proven to have significant impacts on tactical and operational decisions. Furthermore, irrational behaviour in decision-making is not variably detrimental to locomotion efficiency of pedestrians. The proposed framework can serve as an elegant tool to predict pedestrian dynamics. The behavioural findings shed new light on understanding and modelling the tactical and operational decisions in evacuations.**

Manuscript received 18 March 2022; revised 19 September 2022 and 28 November 2022; accepted 12 January 2023. Date of publication 23 January 2023; date of current version 8 May 2023. This work was supported in part by the National Natural Science Foundation of China under Grant 52172362, Grant 52002034, and Grant 52172361; in part by the Major Science and Technology Projects of Shaanxi Province under Grant 2020ZDZX06-01-01; in part by the Fok Yingdong Young Teachers Fund Project under Grant 171103; in part by the Key Research and Development Program of Shaanxi under Grant 2020ZDLGY16-01, Grant 2020ZDLGY16-02, Grant 2020ZDLGY16-03, Grant 2020ZDLGY16-04, and Grant 2021ZDLGY12-01; and in part by the China Scholarship Council under Grant 202006560025. The Associate Editor for this article was H. Dong. *(Corresponding authors: Xuan Zhao; Yufei Yuan.)*

Rong Huang is with the School of Automobile, Chang'an University, Xi'an 710064, China, and also with the Department of Transport and Planning, Delft University of Technology, 2628 CN Delft, The Netherlands (e-mail: huangrong@chd.edu.cn).

Xuan Zhao and Qiang Yu are with the School of Automobile, Chang'an University, Xi'an 710064, China (e-mail: zhaoxuan@chd.edu.cn; qiangyu@chd.edu.cn).

Yufei Yuan and Winnie Daamen are with the Department of Transport and Planning, Delft University of Technology, 2628 CN Delft, The Netherlands (e-mail: Y.Yuan@tudelft.nl; W.Daamen@tudelft.nl).

Chengqing Liu is with CISDI Engineering Company Ltd., CISDI Group Company Ltd., Chongqing 401120, China (e-mail: 1039150916@qq.com).

Digital Object Identifier 10.1109/TITS.2023.3237335

***Index Terms*— Pedestrian simulation, tactical decision, operational decision, cumulative prospect theory, cellular automaton.**

I. Introduction

INCREASING urban population leads to more frequent mass gatherings featured with crowdedness, during which catastrophic disasters may occur due to congestion, especially in emergencies. To facilitate public safety, understanding, estimating and predicting pedestrian evacuation behaviour is of particular importance [1]. With the various advantages (e.g., low cost and no risk) in comparison to experiments, numerical simulations become increasingly popular in pedestrian dynamics research [2]. Different types of microscopic evacuation models have been developed such as force-based models [3], agent-based models [4], and rule-based models [5], [6]. As one type of widely used rule-based models, the floor field cellular automaton (FFCA) model enjoys merits in terms of flexibility, extendibility and computation efficiency [5], [6], and thus has a broad range of applications such as large-scale simulation and real-time prediction [6].

These applications require the FFCA model efficiently and accurately tackle the evacuation behaviour at the strategic, tactical and operational levels [7]. Due to the complicated pre-evacuation activities, it is difficult to precisely model various behaviours at the strategic level [8]. In contrast, the latter two, typically referred to as the exit or route choice behaviour and the locomotion behaviour respectively [9], which have relatively more clarified causation mechanisms and evolution patterns that can be mathematically described, are the focus of this paper. Since an evacuation is essentially a risk event, and pedestrians are unlikely aware of all alternatives and/or corresponding possibilities for each choice during evacuations due to the limited perception ability (i.e., uncertainty), these behaviours concern decision-making under risk and uncertainty [7].

At the tactical and operational levels, utility theory (UT), including expected utility theory (EUT) and random utility theory (RUT), has reigned in the modelling of behaviour decision-making. In this normative theory, it is assumed that all possible outcomes and corresponding attributes are completely known by decision-makers, who are perfectly rational to achieve the maximization of utility [10]. The studies based on UT provide significant insights into certain tactical and operational behaviour patterns and determinants. However,

UT has long been criticized for a series of violations (e.g., bounded rationality and skew risk attitudes) of its basic axioms when employed to describe decision-making under risk and uncertainty [24], [25].

To resolve the major violations of UT, an adequate descriptive theory, Cumulative Prospect Theory (CPT), was proposed [25] [26]. CPT frames the perceived outcomes as gains and losses by a reference point and uses the value function and the weighting function to jointly describe people's choice behaviour under risk and uncertainty. It has been applied to successfully model various travel-related behaviours (e.g., [27]), and some studies indicated that CPT exhibits better performance than EUT in capturing behaviour characteristics (bounded rationality and risk attitudes) of decision-making under risk and uncertainty (e.g., [28], [29]).

In the field of pedestrian dynamics, Mesmer and Bloebaum [13] advocated the need for a behavioural model that can capture pedestrians' preferences on uncertainty in the decision-making process. Recently, bounded rationality and skew risk attitudes (risk-seeking or risk-aversion) have also been observed in experiments [30], [31]. However, in microscopic evacuation models, the risk and uncertainty attributes of tactical and operational decisions have been greatly overlooked, even lacking a methodology to delineate the related decision characteristics (bounded rationality and risk attitudes), let alone their effects on evacuation processes.

To bridge the aforementioned gaps, this paper puts forward an innovative two-layer FFCA model framework composed of three sub-modules (exit choice, locomotion movement and exit-choice changing modules). The main contributions of this paper are as follows:

(1) Two novel behavioural modules based on CPT are proposed to respectively model the exit choice and the locomotion behaviours so that the impact of bounded rationality and risk attitudes on evacuations are encapsulated.

(2) Attractive and repulsive forces are introduced to describe pedestrians' tendency to revisit the original decision in the exit-choice changing module.

(3) The assessment from typical performance metrics demonstrates that the three behavioural modules can reproduce tactical and operational (including locomotion movement and self-organized lane formation) decisions empirically observed in various scenarios, and that CPT-based approach achieves better performance than EUT-based approach (the state-of-the-art approach). Besides, when compared with experiments, the overall degree of match of the results from our locomotion module is higher than that from the state-of-the-art CA model (i.e., a discrete field CA model by Fu et al. [6]). And, the whole framework is further validated using empirical data from three case studies.

(4) The impacts of the decision-making preferences (i.e., the degree of rationality and risk attitudes) on the exit choice and locomotion behaviours are for the first time systematically revealed by a sensitivity analysis.

The structure of this paper is as follows: Section II reviews related works focused on modelling tactical and operational decisions. Section III proposes the FFCA model framework and introduces the key parameters. Section IV calibrates and validates the three sub-modules proposed in Section III by empirical data, followed by sensitivity analyses on the decision-making preference parameters and the validation of the whole framework. Finally, the key findings of this paper and recommendations for future research are concluded in Section V.

II. Related Work

Table I summarizes existing typical studies of tactical and operational decision-making modelling according to the types of approach, the capability of capturing bounded rationality, risk attitudes and lane formation, and the implementation of calibration and validation procedures. For a comprehensive comparison, the proposed framework is also included and assessed, the results of which are presented in bold in Table I.

A. Tactical Decision-Making Modelling

Tactical decision-making refers to the global route/exit choice behaviour [2]. As the pioneers, Hoogendoorn and Bovy [7] proposed a theory and model to describe this behaviour under uncertainty based on UT. Beneficial from the additivity of utility (or disutility) resulting from different factors, one can flexibly incorporate the factors of interest in the utility function. Thus, following a similar methodology (i.e., UT), many models that focus on different factors (e.g., environment, social influence, etc.) related to tactical decision-making have been proposed and estimated (e.g., [11], [12], [13], [14], [15], [16]). Recently, some studies deployed the principle of minimizing time cost to model tactical decisions (e.g., [17], [18]). However, none of them is capable of capturing bounded rationality and risk attitudes in tactical decision-making, let alone revealing their effects.

B. Operational Decision-Making Modelling

Operational decision-making refers to the short-range movement choice behaviour [2]. Amongst many studies using the FFCA model, the logit-based discrete choice model (belonging to RUT) is used to determine the movement choice in each time step (e.g., [5], [6], [19], [20], [21], [22]). However, the traditional logit-based discrete choice model cannot capture the decision-making characteristics in risky and uncertain situations. Recently, to resolve this problem, Gao et al. [23] integrate the CA model with CPT. Since the exit and route choice decision-making is achieved based on operational behaviour in their model, it is essentially an operational-level model according to [2]. In [23], to determine the objective outcomes and occurrence probabilities of alternatives, measurement-based accurate information is used. This operation deviates from the real situations where pedestrians make decisions according to perception-based uncertain information [13]. And, their work did not calibrate the decision-making preference parameters of CPT by empirical evacuation data but relied on the parameter values obtained from studies [25], [26] in economics and psychology, let alone conduct a sensitivity analysis to investigate the effect of each parameter. Moreover, although their

TABLE I
SUMMARY OF THE EXISTING TACTICAL AND OPERATIONAL DECISION-MAKING MODELLING METHODS

Behavioural level	Model name	Approach	Capturing bounded rationality	Capturing risk attitudes	Capturing Lane formation	Calibration	Validation
Tactical	Hoogendoorn and Bovy [7]	UT (EUT)	×	×	-	√	√
	Duives and Mahmassani [11]	UT (RUT)	×	×	-	√	√
	Lovreglio, *et al.* [12]	UT (RUT)	×	×	-	√	√
	Mesmer and Bloebaum [13]	UT (EUT)	×	×	-	×	√
	Liao, *et al.* [14]	UT (RUT)	×	×	-	√	√
	Haghani and Sarvi [15]	UT (RUT)	×	×	-	√	√
	Cao, *et al.* [16]	UT (RUT)	×	×	-	×	×
	Yu [17]	Minimizing defined time cost	×	×	-	×	√
	Wang, *et al.* [18]	Minimizing defined time cost	√	×	-	×	√
	This paper	**CPT**	**√**	**√**	**-**	**√**	**√**
Operational	Burstedde, *et al.* [5]	UT (RUT)	×	×	√	√	√
	Kretz [19]	UT (RUT)	×	×	?	×	√
	Guo, *et al.* [20]	UT (RUT)	×	×	?	×	√
	Suma, *et al.* [21]	UT (RUT)	×	×	√	×	√
	Nowak and Schadschneider [22]	UT (RUT)	×	×	√	×	√
	Fu, *et al.* [6]	UT (RUT)	×	×	?	×	√
	Gao, *et al.* [23]	CPT	√	√	?	×	√
	This paper	**CPT**	**√**	**√**	**√**	**√**	**√**

The symbols identify whether the assessed simulation model implements a specific capability/procedure (√=yes, ×=no, and ?=unproven).

model can describe the conscious locomotion movement, the capability of reproducing lane formation, one of the significant self-organized collective structures in bidirectional flows [2], has so far remained unproven.

C. Summary

To conclude, this review clearly suggests that a calibrated and validated evacuation model framework that has the capability of capturing pedestrians' tactical and operational decision-making preferences is absent in literature, and that the extent to which the decision-making preferences impact evacuations are still unclear. This study fills these gaps by providing the first effort to develop such a framework and uncover the effects of the decision-making preferences. Similar to [23], CPT is used. Nonetheless, the objective outcomes and occurrence probabilities of alternatives in our framework are determined by perception-based uncertain information obtained from a mimicked pedestrian reasoning process [32]. This is a more reasonable and interpretable means, compared to the use of accurate information directly calculated from mathematical functions in [23].

III. MODEL FRAMEWORK DEVELOPMENT

This section presents the modelling process of the proposed FFCA model framework. First, the three sub-modules of the framework, and their key components and parameters are outlined. Next, the exit choice, exit-choice changing and locomotion movement modules are introduced in detail, which are integrated as an overall framework. Later on, the proposed three modules will be calibrated and validated by empirical data.

A. Overview of the FFCA Model Framework

The proposed FFCA model framework is defined on a two-dimension discrete space and dedicated to the normal evacuation situation where pedestrians evacuate as fast as possible, but without pushing. In this context, many factors

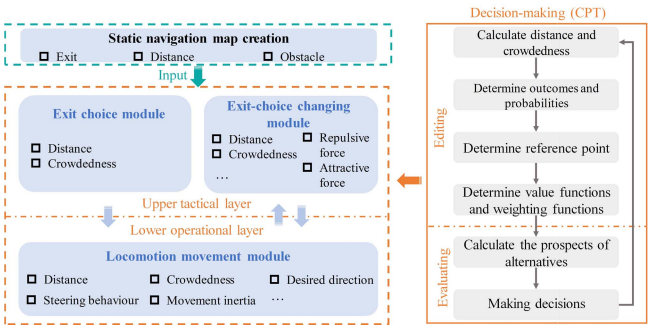

Fig. 1. Overview of the FFCA model framework. In each blue box, the sub-items are the elements considered in the corresponding module. And, each grey box represents a key process or component.

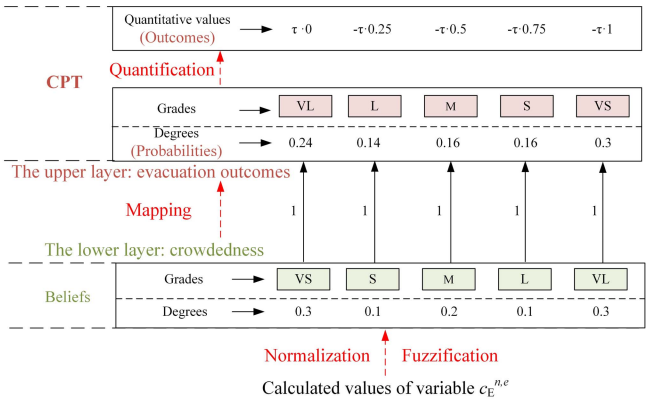

Fig. 2. An example of the information transformation process (variable $c_{\mathrm{E}}^{n,e}$). The outcomes related to $c_{\mathrm{E}}^{n,e}$ are modelled as losses as $c_{\mathrm{E}}^{n,e}$ is disutility for evacuation.

have been demonstrated to impact pedestrian tactical and operational decisions, of which only two factors well validated by empirical observations, i.e., distance and crowdedness [15], are chosen to illustrate the fundamental theories and formulations of the proposed framework. Nevertheless, it can be flexibly extended to incorporate other influential factors related to the evacuation outcome (e.g., fire products) by using the information transformation procedures in this paper.

As shown in Fig. 1, this framework consists of two behavioural layers, i.e., the upper tactical layer and the lower operational layer. The former includes the exit choice and exit-choice changing modules, and the latter corresponds to the locomotion movement module. Based on the environmental information, the algorithm proposed in another work [33] is used to create the static floor field, which provides the static navigation map for decision-making in these three modules. This means that pedestrians are assumed to know the geometric layout (e.g., exits and obstacles) of the environment in our framework, which is the underlying premise of the static floor field algorithm [5], [33].

Once the exit choice is decided, pedestrians begin to conduct the locomotion movement towards the destination. Besides distance and crowdedness, the desired direction, the steering behaviour, the movement inertia and the velocity updating mechanism are also introduced to embody the movement characteristics. In the process of moving to the exit, pedestrians who tend to change the exit choice due to congestion could be given the opportunity to revise the routing decision.

The tactical and operational decisions are modelled by using CPT, characterized by the editing and evaluating phases. Through these two phases, the prospects associated with different alternatives are calculated, based on which pedestrians make decisions. The key notation for the three sub-modules and the integrated framework is illustrated in Table XIV.

B. Tactical-Level Decision Modules

1) Exit Choice Module: The procedure for determining the exit choice is denoted by **EC-Determination**(ST^e, SD^e, α_{E}, β_{E}, λ_{E}, γ_{E}, δ_{E}, $r_{d_{\mathrm{E}}}^n$), shown in Algorithm 1 (see Appendix). More details are illustrated in the ensuing sections.

a) Determining distance and crowdedness: For pedestrian n located in cell (i, j), distance $d_{\mathrm{E}}^{n,e}$ is defined as the distance difference between the maximum distance to evacuate from $\mathbb{C}$ and the distance of pedestrian n to exit e, given by (1).

$$d_{\mathrm{E}}^{n,e} = m_{\mathrm{D}} - D_{\mathrm{C}}^{e,(i,j)} \tag{1}$$

Crowdedness $c_{\mathrm{E}}^{n,e}$ describes the potential resistance of moving to the candidate exits. To avoid the effect of crowd's un-uniform distribution, $c_{\mathrm{E}}^{n,e}$ is determined by weighting path resistance r_{E}^{ne} and density item $\max\left\{\rho_{\mathrm{E}}^{e,1}, \rho_{\mathrm{E}}^{e,2}\right\}$, with consideration of the exit width, shown in (2).

$$c_{\mathrm{E}}^{n,e} = \left(\frac{0.5{\cdot}r_{\mathrm{E}}^{n,e} + 0.5 \cdot \max\left\{\rho_{\mathrm{E}}^{e,1}, \rho_{\mathrm{E}}^{e,2}\right\}}{w_{\mathrm{E}}^{e}}\right) \cdot m_{\mathrm{W}} \tag{2}$$

With

$$r_{\mathrm{E}}^{n,e} = \frac{1}{N(S_{\mathrm{E}}^{n,e})} \sum\nolimits_{(i,j)}^{S_{\mathrm{E}}^{n,e}} \rho^{e,(i,j)} \tag{3}$$

where shortest path cell set $S_{\mathrm{E}}^{n,e}$ is determined by iteratively searching the neighbouring cell along the desired direction (given by (20)-(23)) of each cell from pedestrian n's current location to exit e.

b) Determining outcomes and probabilities: During evacuations, pedestrians receive perception-based uncertain information rather than measurement-based accurate information to judge the variable situations [13]. To reasonably mimic pedestrians' reasoning process, an information transformation process using the techniques common in decision theory [32] is implemented, illustrated in Fig. 2. At the lower level, the fuzzy set theory is applied to transform the calculated $d_{\mathrm{E}}^{n,e}$ and $c_{\mathrm{E}}^{n,e}$ values of each exit to the probabilistic information (a common practice in literature, e.g., [34]). As such, the calculated values are first normalized and then are respectively reframed to the beliefs held by pedestrians, including the grades and the corresponding degrees. Five linguistic grades are considered as they are sufficient to distinguish information with different strengths [34], defined by the Gauss function in (4).

$$f(x) = \exp\left(-\frac{(x-\mu^l)^2}{2\sigma^{l2}}\right) \tag{4}$$

where $x = Norm(d_E)$ or $Norm(c_E)$, and $Norm(y) = y/\max(y)$ represents the normalization operation for vector y; μ^l is the mean related to the linguistic grades ([0, 0.25, 0.5, 0.75, 1] is set for [Very small (VS), Small (S), Medium (M), Large (L) and Very large (VL)] respectively); σ^l is the standard deviation, set as 0.1.

After normalization and fuzzification, a mapping method in [32] is used to transform the uncertain information from the basic attributes in varying utility dimensions (in the lower layer) to the assessment information of a common attribute in the upper layer, so as to generate an overall evaluation for the evacuation efficiency (outcomes) of different options. Intuitively, a farther distance/higher degree of crowdedness means a lower evacuation efficiency. The exactly one-to-one mapping rule between the grades in the lower and upper layers is used, as illustrated in Fig. 2, though the mapping preference may be varied for different pedestrians. The lack of existing knowledge regarding it necessitates such an operation in this exploratory study. However, it does not induce any detriment to the demonstration of the superiority of the proposed model framework.

Finally, each grade j for an attribute i can be quantified by the value $h^{j,i} = h^i_{\max} + \frac{h^i_{\max} - h^i_{\min}}{N(j)-1}(j-1)$ $(j = 1, 2, \ldots, N(j))$ [32], where $h^i_{\min}$ and $h^i_{\max}$ are the minimum and maximum values, and $N(j)$ is the number of grades. Because it is difficult to determine $h^i_{\min}$ and $h^i_{\max}$ in each decision case, using the normalized values becomes a practical operation [32], i.e., $h^i_{\min} = \tau \cdot 0(-\tau \cdot 1)$, and $h^i_{\max} = \tau \cdot 1(\tau \cdot 0)$. The value of τ influences the sensitivity of decision-making to the variances of CPT's parameters, and a sufficiently sensitive response is observed when $\tau = 100$ based on a reiterative try-and-error process. This way, two essential components of CPT, including the evacuation outcomes and corresponding probabilities, can be obtained.

c) Reference point, value function, and weighting function: According to the definition of $d_E^{n,e}$ and $c_E^{n,e}$, they are respectively utility and disutility for evacuation, and thus the related outcomes are modelled as gains and losses respectively. Accordingly, the reference point is set as zero.

The prospect induced by distance and crowdedness is calculated separately using the same procedure, and thus that related to distance is exemplified here to illustrate this process. Assume that pedestrian n is faced with A alternatives (exits), and alternative (exit) e consists of a set of potential outcomes related to distance $o^{n,e,(-q)}_{d_E} < \ldots < o^{n,e,0}_{d_E} < \ldots o^{n,e,t}_{d_E}$, which occur with probability $pr^{n,e,(-q)}_{d_E}, \ldots, pr^{n,e,t}_{d_E}$, respectively. Using a potential outcome j of exit e as an example, the perceived value $(V\left(o^{n,e,j}_{d_E}\right))$ is calculated by (5).

$$V\left(o^{n,e,j}_{d_E}\right) = \begin{cases} \left(\Delta o^{n,e,j}_{d_E}\right)^{\alpha_E} & \Delta o^{n,e,j}_{d_E} = o^{n,e,j}_{d_E} - o^{n,e,0}_{d_E} \geq 0 \\ -\lambda_E\left(-\Delta o^{n,e,j}_{d_E}\right)^{\beta_E} & \Delta o^{n,e,j}_{d_E} = o^{n,e,j}_{d_E} - o^{n,e,0}_{d_E} < 0 \end{cases} \quad (5)$$

where $o^{n,e,j}_{d_E}$ is evacuation outcome j of exit e induced by distance, $o^{n,e,0}_{d_E}$ is the reference point; α_E and β_E determine pedestrians' risk attitudes towards gains and losses respectively; λ_E measures the degree of loss aversion.

The decision weight of potential outcome j is given by (6)

$$\begin{cases} w^+\left(pr^{n,e,j}_{d_E}\right) = \dfrac{\left(pr^{n,e,j}_{d_E}\right)^{\gamma_E}}{\left(\left(pr^{n,e,j}_{d_E}\right)^{\gamma_E} + \left(1 - pr^{n,e,j}_{d_E}\right)^{\gamma_E}\right)^{\frac{1}{\gamma_E}}} \\ if\ \ \Delta o^{n,e,j}_{d_E} \geq 0 \\ w^-\left(pr^{n,e,j}_{d_E}\right) = \dfrac{\left(pr^{n,e,j}_{d_E}\right)^{\delta_E}}{\left(\left(pr^{n,e,j}_{d_E}\right)^{\delta_E} + \left(1 - pr^{n,e,j}_{d_E}\right)^{\delta_E}\right)^{\frac{1}{\delta_E}}} \\ otherwise \end{cases} \quad (6)$$

where w^+ and w^- represent the cumulative weighting function for gains and losses, respectively; $pr^{n,e,j}_{d_E}$ is the occurrence probability of $o^{n,e,j}_{d_E}$; γ_E and δ_E reflect the degree of distortion in subjective judgments of the occurrence probabilities of gains and losses respectively.

Then, the cumulative prospect values $(P^{n,e}_{d_E})$ induced by distance is calculated by (7)

$$P^{n,e}_{d_E} = P^{n,e,+}_{d_E} + P^{n,e,-}_{d_E} \quad (7)$$

With

$$P^{n,e,+}_{d_E} = \sum\nolimits_{j=0}^{t} \pi^{n,e,j,+}_{d_E} \cdot V\left(o^{n,e,j}_{d_E}\right) \quad (8)$$

$$P^{n,e,-}_{d_E} = \sum\nolimits_{j=-q}^{0} \pi^{n,e,j,-}_{d_E} \cdot V\left(o^{n,e,j}_{d_E}\right) \quad (9)$$

where $P^{n,e,+}_{d_E}$ and $P^{n,e,-}_{d_E}$ are the prospect of gains and losses for exit e respectively; π^+ and π^- are the decision weights for gains and losses respectively, given by (10)-(13).

$$\pi^{n,e,(-q),-}_{d_E} = w^-\left(pr^{n,e,(-q)}_{d_E}\right) \quad (10)$$

$$\pi^{n,e,j,-}_{d_E} = w^-\left(pr^{n,e,(-q)}_{d_E} + \ldots + pr^{n,e,j}_{d_E}\right) - w^-\left(pr^{n,e,(-q)}_{d_E} + \ldots + pr^{n,e,(j-1)}_{d_E}\right), \quad 1 - q \leq j \leq 0 \quad (11)$$

$$\pi^{n,e,j,+}_{d_E} = w^+\left(pr^{n,e,j}_{d_E} + \ldots + pr^{n,e,t}_{d_E}\right) - w^+\left(pr^{n,e,(j+1)}_{d_E} + \ldots + pr^{n,e,t}_{d_E}\right), \quad 0 \leq j \leq t - 1 \quad (12)$$

$$\pi^{n,e,t,+}_{d_E} = w^+\left(pr^{n,e,t}_{d_E}\right) \quad (13)$$

In the CPT, α_E, β_E, λ_E, γ_E and δ_E control the degree of rationality. A greater deviation of α_E, β_E, λ_E, γ_E and δ_E from 1 (perfect rationality) is, a higher degree of irrationality it is for decision-makers. Also, α_E and β_E reflect the risk preference. For gains/losses, a greater negative and positive deviation of α_E/β_E from 1 (risk-neutral) indicates a greater degree of risk-aversion/risk-seeking and risk-seeking/risk-aversion respectively. When $\alpha_E = \beta_E = \lambda_E = \gamma_E = \delta_E = 1$, CPT turns into EUT, and thus it is a special version of CPT. This allows a convenient performance comparison between CPT and EUT in the proposed exit choice and locomotion movement modules. The value of the decision-making preference parameters will be determined by calibration using empirical data.

d) Exit choice decision: Pedestrian n makes the decision according to the synthetic prospect of exit e, calculated by (14)

$$P_{\mathrm{E}}^{n,e} = r_{c_{\mathrm{E}}}^{n} \cdot P_{c_{\mathrm{E}}}^{n,e} + r_{d_{\mathrm{E}}}^{n} \cdot P_{d_{\mathrm{E}}}^{n,e} \tag{14}$$

where $r_{c_{\mathrm{E}}}^{n}$ and $r_{d_{\mathrm{E}}}^{n}$ are the proportion coefficients of prospect values $P_{c_{\mathrm{E}}}^{n,e}$ and $P_{d_{\mathrm{E}}}^{n,e}$ for pedestrian n respectively, and $r_{c_{\mathrm{E}}}^{n} + r_{d_{\mathrm{E}}}^{n} = 1$; $P_{c_{\mathrm{E}}}^{n,e}$ and $P_{d_{\mathrm{E}}}^{n,e}$ denote the prospect value resulting from variables $d_{\mathrm{E}}^{n,e}$ and $c_{\mathrm{E}}^{n,e}$ for exit e, respectively.

Considering pedestrians' cognitive errors, the probability of choosing exit e is determined by the multinomial logit model, shown in (15).

$$\mathcal{P}_{\mathrm{E}}^{n,e} = \frac{\exp\left(P_{\mathrm{E}}^{n,e}\right)}{\sum_j \exp\left(P_{\mathrm{E}}^{n,j}\right)} \tag{15}$$

2) Exit-Choice Changing Module: Although the exit-choice changing behaviour is generally infrequent as observed in real crowds [14], it is critically important for accurate and realistic pedestrian evacuation simulations [35]. And thus a novel method is proposed to allow the exit-choice changing behaviour, described in Algorithm 2 (see Appendix), denoted by **ECC-Determination**(ST^e, SD^e, $N^{n,e,0}$, N_{O}^{n}, $N_{\mathrm{EV}}^{n,t}$, $t_{\mathrm{BM}}^{n,e}$, N_{EC}^{n}, t, C_{R}, C_{A}).

To avoid unrealistically frequent exit-choice changing behaviour, for each pedestrian n, the exit-choice changing module is only activated after the locomotion movement towards target exit e has begun, expressed as (16).

$$\begin{cases} t_{\mathrm{BM}}^{n,e} \neq 0 \\ t_{\mathrm{BM}}^{n,e} < t \end{cases} \tag{16}$$

To quantitatively depict pedestrians' tendency of maintaining or changing the original exit choice, two contradictory elements, i.e., attractive and repulsive forces, are introduced.

The attractive force describes the stickiness to the original decision, which is jointly determined by the relative distance to target exit e $\left(1 - \frac{D_{\mathrm{P}}^{n,e,t}}{M(SD^e)}\right)$ and the flow capacity $\left(1 - \frac{N^{n,e,t}}{N^{n,e,0}}\right)$, shown in (17).

$$A^{n,e,t} = C_{\mathrm{A}} \cdot \left(\left(1 - \frac{D_{\mathrm{P}}^{n,e,t}}{M\left(SD^e\right)}\right) \Big/ 2 + \left(1 - \frac{N^{n,e,t}}{N^{n,e,0}}\right) \Big/ 2\right)^3 \tag{17}$$

The repulsive force consists of three components, determined by (18).

$$R^{n,e,t} = (C_{\mathrm{R}})^{\left(1+N_{\mathrm{EC}}^{n}\right)^2} \cdot \left(1 - \exp\left(-f\left(\frac{N_{\mathrm{EV}}^{n,t}}{N_{\mathrm{O}}^{n}}\right) \cdot G_{\mathrm{R}}^{n,e,t}\right)\right) \tag{18}$$

With

$$G_{\mathrm{R}}^{n,e,t} = \frac{\left(c_{\mathrm{E}}^{n,e} - \min\left(c_{\mathrm{E}}^{n,e}\right)\right)}{c_{\mathrm{E}}^{n,e}} \tag{19}$$

where $f(x) = x$, if $x < 1$; 1, otherwise.

The first component is $G_{\mathrm{R}}^{n,e,t}$, which quantifies the crowdedness level of target exit e relative to the least congested exit. Intuitively, pedestrian n's tendency of changing the exit decision becomes larger as $G_{\mathrm{R}}^{n,e,t}$ increases. And, pedestrian n is increasingly sensitive to the change of $G_{\mathrm{R}}^{n,e,t}$ as the number of evacuated pedestrians known by pedestrian n increases. This is described by coefficient $f\left(\frac{N_{\mathrm{EV}}^{n,t}}{N_{\mathrm{O}}^{n}}\right)$. Moreover, a penalty factor for changing the decision, $\left(1 + N_{\mathrm{EC}}^{n}\right)^2$, is introduced to avoid frequent re-selection as empirical observations suggest the infrequence of decision change in evacuations.

Finally, pedestrian n has a probability of $(R^{n,e,t} - A^{n,e,t})$ to revise the exit choice. Since it is physically impossible for pedestrians trapped inside a crowd to change the exit, pedestrian n is allowed to make a decision change only when he/she is potentially capable of moving towards the updated exit. This trigger condition is described by a density criterion [35] (i.e., $D_{\mathrm{L}}^{n,e,t} < 3$ ped/m^2).

C_{R} and C_{A} are the two key parameters of this module, which will be calibrated by empirical data in the next section.

C. Locomotion Movement Module

After determining the aimed exit, each pedestrian can move to one of its unoccupied neighbouring cells or stay still in each time step. To allow the diagonal movement of pedestrians, the Moore neighbourhood is used. Pedestrians' locomotion decisions are updated parallelly in each time step [5]. The procedure of this module is depicted in Algorithm 3 (see Appendix), denoted by **LM-Determination**(ST^e, SF^e, α_{M}, β_{M}, λ_{M}, γ_{M}, δ_{M}, $r_{d_{\mathrm{M}}}^{n}$, t). More details are delineated underneath.

1) Determining the Desired Direction: In evacuation models, it is a common practice to assume that pedestrians head towards the direction that makes them closer to the destination (e.g., [3]), which is referred to as the desired direction, determined by (20)-(21).

$$\vec{D}_{\mathrm{C}}^{(i,j)} = \begin{cases} \dfrac{\left(F_{\mathrm{C}}^{e,(i+1,j)} - F_{\mathrm{C}}^{e,(i-1,j)},\, F_{\mathrm{C}}^{e,(i,j+1)} - F_{\mathrm{C}}^{e,(i,j-1)}\right)}{\left\|\left(F_{\mathrm{C}}^{e,(i+1,j)} - F_{\mathrm{C}}^{e,(i-1,j)},\, F_{\mathrm{C}}^{e,(i,j+1)} - F_{\mathrm{C}}^{e,(i,j-1)}\right)\right\|_2} \\ \quad if\ \ N\left(\Omega_{\mathrm{NC}}\right) = 8 \\ \dfrac{(x_{\min} - i,\, y_{\min} - j)}{\|(x_{\min} - i,\, y_{\min} - j)\|_2} \\ \quad otherwise \end{cases} \tag{20}$$

$$\vec{D}_{\mathrm{A}}^{(i,j)} = \arg\min_{k} \left\{\vec{D}_{\mathrm{C}}^{(i,j)} \cdot \vec{D}^{k} \mid k = 1, 2, \ldots, 8\right\} \tag{21}$$

With

$$(x_{\min}, y_{\min}) = \arg\min_{x^l, y^l} \left\{\sqrt{(x^l - i)^2 + (y^l - j)^2} \mid \left(x^l, y^l\right)\right\} \tag{22}$$

$$\left(x^l, y^l\right) = \arg\max_{x^k, y^k} \left\{F_{\mathrm{C}}^{e,(x^k, y^k)} \mid \left(x^k, y^k\right) \in \Omega_{\mathrm{NC}}\right\} \tag{23}$$

where Ω_{NC} is the set of cell (i, j)'s available neighbouring cells. Due to the discreteness of space, the calculated desired direction $\vec{D}_{\mathrm{C}}^{(i,j)}$ is converted to the actual desired direction $\vec{D}_{\mathrm{A}}^{(i,j)}$.

2) Steering to the Desired Direction: At time step t, each pedestrian n located in cell (i, j) has a probability to change its orientation to $\vec{D}_{\mathrm{A}}^{(i,j)}$. The steering probability $P_{\mathrm{S}}^{n,t}$ is given by (24).

$$P_{\mathrm{S}}^{n,t} = \frac{\omega^n \cdot S_{\mathrm{L}}}{v_{\max} \cdot arccos\left(\frac{\vec{D}^{n,t-1} \cdot \vec{D}_{\mathrm{A}}^{(i,j)}}{\|\vec{D}^{n,t-1} \cdot \vec{D}_{\mathrm{A}}^{(i,j)}\|_2}\right)} \tag{24}$$

In addition to a positive correlation with the pedestrian angular speed, $P_{\mathrm{S}}^{n,t}$ decreases with increasing steering angle, which accords with the fact that the greater the angle, the longer it takes for pedestrians to steer.

3) Updating the movement velocity: Pedestrian n will adjust the velocity to accommodate to the changing environment at time step t. This is implemented by (25) [40].

$$v^{n,t} = v_{\mathrm{F}}^n \cdot \left(1 - \exp\left(-r \cdot \left(\frac{1}{\rho^{n,t}} - \frac{1}{\rho_{\max}}\right)\right)\right) \tag{25}$$

where r=1.913 is a factor; $\rho^{n,t}$ is the density within a circular area with pedestrian n as the centre and a radius of L_{SZ} at time step t, and $\rho_{\max} = \frac{1}{S_{\mathrm{L}}^2}$ persons/m^2 is the maximum density.

The updated velocity determines the movement probability $(v^{n,t}/v_{\max})$ of pedestrian n at the current time step.

4) Determining Distance and Crowdedness: For each candidate movement direction $\vec{D}^k$ with the neighbouring cell reachable by pedestrian n, distance $d_{\mathrm{M}}^{n,k}$ is determined by (26).

$$d_{\mathrm{M}}^{n,k} = \frac{1}{N\left(\Omega_{\mathrm{SZ}}^{n,k}\right)} \sum\nolimits_{\left(x_{\mathrm{SZ}}^{n,k}, y_{\mathrm{SZ}}^{n,k}\right) \in \Omega_{\mathrm{SZ}}^{n,k}} F_{\mathrm{C}}^{e,\left(x_{\mathrm{SZ}}^{n,k}, y_{\mathrm{SZ}}^{n,k}\right)} \tag{26}$$

Crowdedness $c_{\mathrm{M}}^{n,k}$ is the arithmetic sum of three components, two cell-level movement resistance elements ($c_{\mathrm{M}}^{n,k,1}$ and $c_{\mathrm{M}}^{n,k,2}$) in the short-range visual zone, and a lane-level movement resistance element ($c_{\mathrm{M}}^{n,k,3}$) in the long-range anticipation zone.

$c_{\mathrm{M}}^{n,k,1}$ and $c_{\mathrm{M}}^{n,k,2}$ identify which cell (direction) is less crowded to guide pedestrians to manoeuvre through dense crowds, calculated by (27)-(28), shown at the bottom of the next page, where $\mathcal{T}$=1, if $\left(x_{\mathrm{SZ}}^{n,k}, y_{\mathrm{SZ}}^{n,k}\right)$ is occupied by a pedestrian; 0, otherwise. $\mathcal{T}'$=1, if $\left(x_{\mathrm{SZ}}^{n,k}, y_{\mathrm{SZ}}^{n,k}\right)$ is occupied by pedestrian n'; 0, otherwise. $\omega^{n,n'} = arccos\left(\frac{\vec{D}^{n,t} \cdot \vec{D}^{n',t}}{\left\|\vec{D}^{n,t} \cdot \vec{D}^{n',t}\right\|_2}\right)$.

$c_{\mathrm{M}}^{n,k,3}$ reflects another common operation of pedestrians, that is, they estimate the potential movement route of others in front to adjust the aimed movement lane for avoiding prospective collisions in advance, calculated by (29).

$$c_{\mathrm{M}}^{n,k,3} = \frac{1}{N\left(\Omega_{\mathrm{LZ}}^{n,\ell}\right)} \sum\nolimits_{\left(x_{\mathrm{LZ}}^{n,\ell}, y_{\mathrm{LZ}}^{n,\ell}\right) \in \Omega_{\mathrm{LZ}}^{n,\ell}} \times \frac{\sum_{n=1}^{L_{\mathrm{LZ}}/S_{\mathrm{L}}} \lambda_{\mathrm{LZ}}^{n \cdot S_{\mathrm{L}}} \cdot \mathcal{T}'' \cdot \frac{\omega^{n,n''}}{\pi} \cdot sign\left(\omega^{n,n''}\right)}{\sum_{n=1}^{L_{\mathrm{LZ}}/S_{\mathrm{L}}} \lambda_{\mathrm{LZ}}^{n \cdot S_{\mathrm{L}}}} \tag{29}$$

With

$$\left(x_{\mathrm{LZ}}^{n,\ell}, y_{\mathrm{LZ}}^{n,\ell}\right) = (i, j) + \Theta \cdot \vec{\nu} \tag{30}$$

where $\mathcal{T}'' = 1$, if $\left(x_{\mathrm{LZ}}^{n,\ell} + n \cdot x^{\vec{D}^{n,t}}, y_{\mathrm{LZ}}^{n,\ell} + n \cdot y^{\vec{D}^{n,t}}\right)$ is occupied by pedestrian n''; 0, otherwise. $sign\left(\omega^{n,n''}\right) = \omega^{n,n''}$, if $\frac{\pi}{2} \leq \omega^{n,n''}$; 0, otherwise. $\omega^{n,n''} = arccos\left(\frac{\vec{D}^{n,t} \cdot \vec{D}^{n'',t}}{\left\|\vec{D}^{n,t} \cdot \vec{D}^{n'',t}\right\|_2}\right)$. $n \in \mathbb{Z}^+$, $\Theta \leq L_{\mathrm{SZ}}/S_{\mathrm{L}}$ and $\Theta \in \mathbb{Z}^+$. $\vec{\nu}$ is a vector solved by equation constraints (see Algorithm 3 in Appendix).

5) Locomotion Decision: For candidate movement direction $\vec{D}^k$, once distance ($d_{\mathrm{M}}^{n,k}$) and crowdedness ($c_{\mathrm{M}}^{n,k}$) are determined, the prospect values can be calculated using the aforementioned procedures.

Then, pedestrian n makes the locomotion decision according to the prospect values of the candidate directions, with a tendency of following others and moving towards the desired direction. Due to the inertia effect, the walking velocity decreases when pedestrians move towards a direction that deviates from the desired direction. A function in [36] is used to describe this characteristic, shown in (31).

$$w_{\mathrm{M}}^{n,k} = \exp\left(-0.09\,|\theta_1|\right) \tag{31}$$

where $\theta^1 \in [-\pi, \pi]$ is the angle (in radians) between $\vec{D}^{n,t}$ and $\vec{D}^k$.

Thus, the movement probability is determined by (32).

$$\begin{cases} w_{\mathrm{M}}^{n,k} \cdot \mathcal{P}_{\mathrm{M}}^{n,k} & \text{Moving towards } \vec{D}^k \\ 1 - \sum_k \mathcal{P}_{\mathrm{M}}^{n,k} & \text{Staying still} \end{cases} \tag{32}$$

With

$$\mathcal{P}_{\mathrm{M}}^{n,k} = \frac{\exp\left(P_{\mathrm{M}}^{n,k} + K_{\mathrm{DF}} \cdot DF^k\right)}{\sum_k \exp\left(P_{\mathrm{M}}^{n,k} + K_{\mathrm{DF}} \cdot DF^k\right)} \tag{33}$$

$$P_{\mathrm{M}}^{n,k} = r_{d_{\mathrm{M}}}^n \cdot P_{d_{\mathrm{M}}}^{n,k} + r_{c_{\mathrm{M}}}^n \cdot P_{c_{\mathrm{M}}}^{n,k} \tag{34}$$

where $r_{d_{\mathrm{M}}}^n$ and $r_{c_{\mathrm{M}}}^n$ are the weights of variables $d_{\mathrm{M}}^{n,k}$ and $c_{\mathrm{M}}^{n,k}$ respectively, and $r_{d_{\mathrm{M}}}^n + r_{c_{\mathrm{M}}}^n = 1$; $P_{d_{\mathrm{M}}}^{n,k}$ and $P_{c_{\mathrm{M}}}^{n,k}$ are the prospects resulting from variables $d_{\mathrm{M}}^{n,k}$ and $c_{\mathrm{M}}^{n,k}$ respectively; K_{DF} is the sensitivity parameter of the dynamic field, and DF^k is the dynamic field value of $\vec{D}^k$.

If the target cell is occupied by other pedestrians, pedestrian n will stay still. In case of conflicts where more than one pedestrian target a cell, one of pedestrians is randomly selected to implement the movement.

D. The Integrated FFCA Model Framework

The proposed three sub-modules are integrated as a FFCA model framework, denoted as **FFCA**(N_{O}, $\mathbb{C}$) (see Algorithm 4 in Appendix). In the next section, the three sub-modules and the whole framework will be calibrated and validated by empirical data.

IV. Simulation Setups and Results

We performed simulations of case studies for the three sub-modules and also the integrated FFCA model framework under the five basic assumptions unless specified otherwise. First, each pedestrian occupies one cell, and the size of

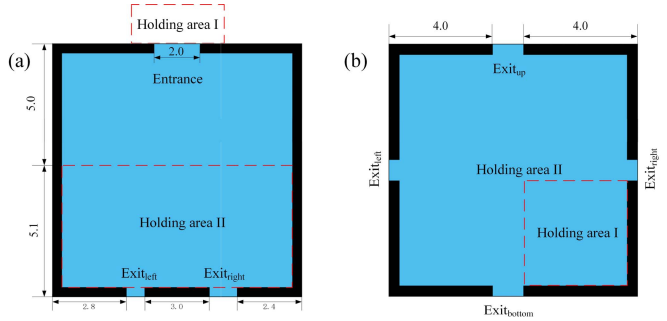

Fig. 3. Physical setups of series A (a) and B (b) experiments used in the simulations of tactical-level decision modules. The black grids denote obstacles and walls. The red dashed box denotes the holding area where the participants are distributed.

each cell is set as 0.4 m × 0.4 m (S_L=0.4), which corresponds to the typical area occupied by a pedestrian in real crowds [37]. Second, the hard core exclusion principle is followed [38], i.e., overlapping between pedestrians and/or obstacles is unallowable. Third, due to the lack of individual decision-making empirical data, the homogeneity of crowds is assumed so as to represent all pedestrians' decision-making preferences by one set of values in this work [28]. Forth, the free velocities of pedestrians follow the normal distribution $v_F^n \sim N(1.34, 0.34^2)$, and K_{DF} is set as 0. Fifth, according to the previous works [26], [39], [40] and the prior simulations, the initial range of each parameter before calibration is set as follows: α_E/α_M and $\beta_E/\beta_M \in (0, 2]$, $\lambda_E/\lambda_M \in [1, 3]$, γ_E/γ_M and $\delta_E/\delta_M \in (0, 1]$, $r^n_{d_E}/r^n_{d_M} \in [0, 1]$, and C_R and $C_A \in [0, 1]$. These assumptions have been widely recognized and used in existing studies (e.g., [5], [6], [28], [33], [38]).

Moreover, based on a preliminary analysis using the principle in [41], 30 runs will be repeated for each simulation to ensure that any difference in simulations with varying parameters is not incurred by the stochasticity of the model. The ensuing section presents the simulation setups and results of the case studies.

A. Simulation Setups

The proposed framework is coded into MATLAB R2021b. A desk computer with an Intel Core i5, 3.1 GHz processor and 6 GB of RAM is used to perform the simulations. Table II presents an overview of the key parameters and the simulations related to each parameter. As an efficient optimization method, the genetic algorithm (GA) is respectively used to search the parameter values with the minimum predefined error in the three sub-modules [42]. The GA is terminated when the goodness-of-fit has little improvement (i.e., less than 0.001) for consecutive 10 rounds. 10 runs with different seeds of initial chromosomes are repeated [42], [43]. The same optimal parameter set is obtained in all the simulation runs, which indicates the robustness of the optimization results. In the later sensitivity analysis, all the decision-making preference parameters except the one to be tested are kept as the calibrated value. Moreover, as the tactical decisions are jointly determined by the exit choice and exit-choice changing modules, they will be calibrated and validated together. According to the well-established principles in [16], [45], and [47], the assessment metrics and the scenarios used in the calibration, validation, and simulation analyses are determined, as illustrated in the ensuing parts.

1) Tactical-Level Decision Modules: Experiment runs A_1∼A_10 and B_1∼B_6 originally presented in [14] for understanding the route choice behaviour are simulated. To determine the locomotion decisions in simulations, the locomotion movement module that is calibrated and validated in the latter section is used. Details related to these two series of experiments are shown in Fig. 3 and Table III. The experimental data processed by Liao et al. [14] are publicly available and thus directly used in this paper. The different experiment runs with similar initial conditions (i.e., A_1∼A_2 and A_3∼A_8) are regarded as one experiment, and finally 10 experiments (indicated by T_1 to T_10) are obtained, see Table III. To ensure the same initial condition between experiments and simulations, the initial positions of participants in holding area I and the flow pattern over time of participants in holding area II are extracted from the trajectory data and fed into the framework.

Although this paper aims to obtain a generic parameter set that is applicable to different scenarios, pedestrians in experiments T_6∼T_8 and the remaining experiments are found to exhibit systematically different decision-making characteristics in prior simulations. Thus, the 10 experiments are classified into two sets, and the calibration and validation of the tactical-level decision modules are separately conducted on

each experiment set, see Table III. Two experiments in set 1 and five experiments in set 2 are used for calibration and the remaining experiment(s) for validation and performance comparisons with the module using EUT (see Table III).

In the tactical-level modules, eight parameters are calibrated, shown in Table II. The performance of each parameter set is assessed by the squared error resulting from

$$c_M^{n,k,1} = \frac{\sum_{\left(x_{SZ}^{n,k}, y_{SZ}^{n,k}\right)\in\Omega_{SZ}^{n,k}} \exp\left(-\left\|\left(i - x_{SZ}^{n,k}, j - y_{SZ}^{n,k}\right)\right\|_2 \Big/ L_{SZ}\right)\cdot \mathcal{T}}{\sum_{\left(x_{SZ}^{n,k}, y_{SZ}^{n,k}\right)\in\Omega_{SZ}^{n,k}} \exp\left(-\left\|\left(i - x_{SZ}^{n,k}, j - y_{SZ}^{n,k}\right)\right\|_2 \Big/ L_{SZ}\right)} \tag{27}$$

$$c_M^{n,k,2} = \frac{\sum_{\left(x_{SZ}^{n,k}, y_{SZ}^{n,k}\right)\in\Omega_{SZ}^{n,k}} \exp\left(-\left\|\left(i - x_{SZ}^{n,k}, j - y_{SZ}^{n,k}\right)\right\|_2 \Big/ L_{SZ}\right)\cdot \mathcal{T}'\cdot \omega^{n,n'}}{\sum_{\left(x_{SZ}^{n,k}, y_{SZ}^{n,k}\right)\in\Omega_{SZ}^{n,k}} \exp\left(-\left\|\left(i - x_{SZ}^{n,k}, j - y_{SZ}^{n,k}\right)\right\|_2 \Big/ L_{SZ}\right)} \tag{28}$$

TABLE II

PARAMETERS AND THE RELATED SIMULATIONS IN THE TACTICAL AND OPERATIONAL DECISION MODULES

Type	Symbol	Meaning	Tactical			Operational		
			Cal	Val	SS	Cal	Val	SS
Decision-making preference parameters (CPT)	α_E/α_M	Risk attitude towards gains	√	√	√	√	√	√
	β_E/β_M	Risk attitude towards losses	√	√	√	√	√	√
	λ_E/λ_M	Degree of loss aversion	√	√	√	√	√	√
	γ_E/γ_M	Distortion in judging probability of gains	√	√	√	√	√	√
	δ_E/δ_M	Distortion in judging probability of losses	√	√	√	√	√	√
Other module parameters	$r_{d_E}^n/r_{d_M}^n$	Weight of distance prospects	√	√		√	√	
	C_R	Repulsive force coefficient	√	√		-	-	-
	C_A	Attractive force coefficient	√	√		-	-	-

The acronyms identify the conducted simulations (i.e., Cal=calibration, Val=validation, and SS=sensitivity analysis)

TABLE III

DETAILS RELATED TO SERIES A AND B EXPERIMENTS [14] USED IN THE SIMULATIONS OF TACTICAL-LEVEL DECISION MODULES

Set	Setup	Original name in [14]	Purpose	N_I	N_{II}	$\text{Exit}_{\text{left}}$ (m)	$\text{Exit}_{\text{right}}$ (m)	Exit_{up} (m)	$\text{Exit}_{\text{bottom}}$ (m)
1	T_6	B_2	VC and SS	40	0	0.8	0.8	0.8	0.8
	T_7	B_3	Cal	40	0	0.8	0.8	0.8	0.8
	T_8	B_4	Cal	40	0	0.8	0.8	0.8	0.8
2	T_1	A_1~A_2	Cal	18	0	0.7 (0.8*)	1.1 (1.2*)	-	-
	T_2	A_3~A_8	Cal	40	0	0.7 (0.8*)	1.1 (1.2*)	-	-
	T_3	A_9	Cal	48	90	0.7 (0.8*)	1.1 (1.2*)	-	-
	T_4	A_10	VC and SS	48	90	0.7 (0.8*)	1.1 (1.2*)	-	-
	T_5	B_1	Cal	11	0	0.8	0.8	0.8	0.8
	T_9	B_5	Cal	0	138	0.8	0.8	1.2	1.2
	T_10	B_6	VC and SS	0	138	0.8	0.8	1.2	1.2

The acronyms identify the purposes (i.e., VC=validation and comparison, Cal=calibration and SS=sensitivity analysis). N_I and N_{II} are respectively the number of participants in holding areas I and II. Asterisk sign (*) indicates the exit width values actually used in simulations due to the discreteness of space.

TABLE IV

DETAILS RELATED TO THE EXPERIMENTS [44] USED IN THE SIMULATIONS OF THE LOCOMOTION MOVEMENT MODULE

Setup	Purpose	Original name in [44]	Scenario	Density variant	b_C (m)	b_E (m)	N (N_L/N_R)
M_1	Cal	AO-360-400	Bo	High	-	3.6	400
M_2	Cal	BO-360-160-160	Bi	High	3.6	-	300 (150/150)
M_3	Cal	EO-240-150-240	Co	High	2.4	-	100
M_4	VC and SS	AO-440-400	Bo	High	-	4.4	400
M_5	VC	AO-240-350	Bo	High	-	2.4	400
M_6	VC and SS	BO-360-120-120	Bi	High	3.6	-	200 (100/100)
M_7	VC	BO-360-075-075	Bi	Low	3.6	-	100 (50/50)
M_8	VC and SS	EO-240-100-240	Co	High	2.4	-	100
M_9	VC	EO-240-060-240	Co	Low	2.4	-	50

b_C and b_E are the dimension parameters of the experimental setups, shown in Fig. 4. N is the total number of participants. N_L and N_R are the number of participants entering into the corridor from a waiting area in its left and right sides respectively.

three aspects that include six metrics affected by tactical decisions, i.e., two metrics for the exit choice behaviour: the **exit shares (ES)** and the **individual-level exit choice matching proportion (IEMP)**, two metrics for the exit-choice changing behaviour: the **average timing of changing the exit choice (ATCE)**and the **frequency of changing the exit choice (FCE)**, and two metrics for the whole evacuation process: the **total evacuation time (TET)** and the **mean of individual**

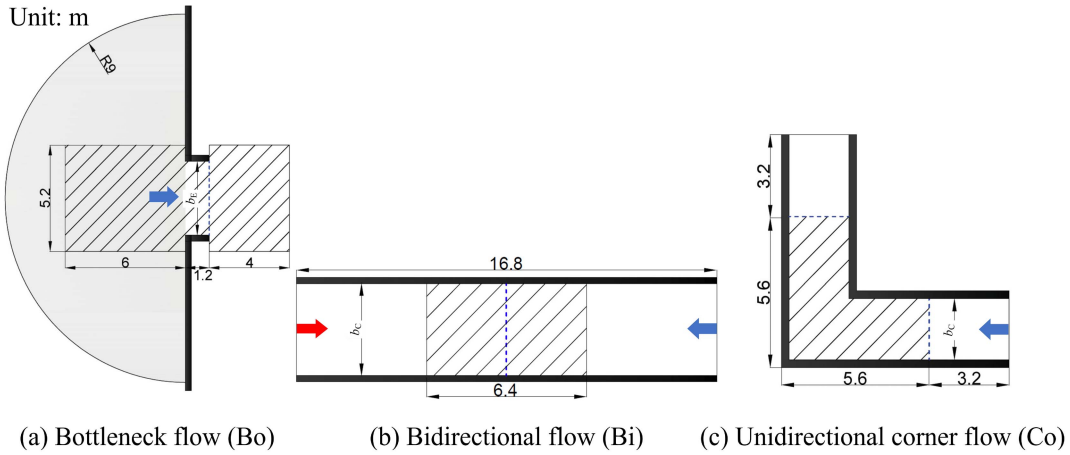

(a) Bottleneck flow (Bo) (b) Bidirectional flow (Bi) (c) Unidirectional corner flow (Co)

Fig. 4. Layout of the three movement scenarios used in the simulations of the locomotion movement module. The hatched areas represent the measurement areas; the dashed blue lines indicate the location where the FR is measured and the grey area in (a) indicates the waiting area of pedestrians; the red and blue arrows indicate the flow directions.

evacuation times (MIET). Specifically, IEMP measures the average degree of match between simulations and experiments in terms of individual exit choices and thus is a mesoscopic metric. The timing of changing the exit choice is defined as the ratio of the time until a pedestrian changes the exit to his/her total evacuation time. The final objective is formulated as (35) using the weighted sum method [48].

$$\mathrm{dist_E} = \frac{1}{N_\mathrm{E}^1 N_\mathrm{E}^2} \sum\nolimits_{i=1}^{N_\mathrm{E}^1} \sum\nolimits_{j=1}^{N_\mathrm{E}^2} \mathrm{dist}_\mathrm{E}^{i,j} \tag{35}$$

where N_E^1 and N_E^2 are respectively the number of the experiments and the assessment aspects; $\mathrm{dist}_\mathrm{E}^{i,j}$ is the average normalized squared error of the two metrics from aspect j for experiment i, calculated by (36).

$$\mathrm{dist}_\mathrm{E}^{i,j} = \frac{1}{2} \cdot \left(\frac{M_\mathrm{sim}^{i,j,1} - M_\mathrm{exp}^{i,j,1}}{M_\mathrm{norm}^{i,j,1}} \right)^2 + \frac{1}{2} \cdot \left(\frac{M_\mathrm{sim}^{i,j,2} - M_\mathrm{exp}^{i,j,2}}{M_\mathrm{norm}^{i,j,2}} \right)^2 \tag{36}$$

where M_sim and M_exp are respectively the simulated and observed values of the metric, and superscripts 1 and 2 respectively represent the two metrics related to aspect j; M_norm is the value used for normalization [47]. Specifically, for IEMP, $M_\mathrm{exp} = 1$, and $M_\mathrm{sim} = \frac{1}{N_\mathrm{P}^i} \sum_{k=1}^{N_\mathrm{P}^i} \frac{N_\mathrm{M}^{i,k}}{N_\mathrm{R}}$, where N_P^i is the number of pedestrians in experiment i, N_R is the number of simulation runs, and $N_\mathrm{M}^{i,k}$ is the number of simulation runs where pedestrian k's exit choice is matched with that in experiment i.

After calibration and validation, setups T_4, T_6 and T_10 (one experiment for each type of physical setups or pedestrian distributions) are used to investigate the impact of the decision-making preferences on the exit choice behaviour based on metrics ES and IEMP in a sensitivity analysis (see Tables II and III). Through these analyses, we aim to determine whether these two sub-modules can well describe the tactical decisions in real life and to which extent CPT performs better than EUT in respect of mimicking the exit choice behaviour, and to reveal how the decision-making preferences influence the exit choice behaviour.

2) Locomotion Movement Module: To calibrate and validate this module, three movement scenarios from the HERMES project [44], i.e., a bottleneck flow, a bidirectional flow and a unidirectional corner flow, are chosen so as to cover pedestrian movement behaviour in different traffic infrastructures [2], [46]. To reduce the computational burden, for each scenario, only a high density variant is selected for calibration, as suggested in [46], see Table IV. In the later validation and performance comparisons with the module using EUT and the model of Fu et al. [6], both the high and low density variants of each scenario (except for the bottleneck flow scenario which only has a high density variant) are used to comprehensively assess the model performance at the situations with different density levels, see Table IV. Correspondingly, Fig. 4 shows an overview of the layout of the scenarios used in simulation analyses.

The measures suggested by [47] are conducted to ensure a similar initial condition between simulations and experiments (e.g., flow pattern over time). Moreover, in setups M_2 and M_6, K_DF is set to 0.3, and it is 0.8 in setup M_7. This is because in a lower density scenario a stronger herding tendency is needed for pedestrians to follow the persons' steps in front.

Using the GA, six parameters are calibrated (see Table II). The fitness of each parameter set is comprehensively assessed by three movement metrics (two macro-level metrics: the flow rate (FR) and the density distribution (DD), one meso-level metric: the travel time distribution (TTD)) [46] and one self-organization phenomenon metric (one macro-level metric: average order parameter (AOP)) [49].

Flow rate (FR). it is the average flow rate (in p/s/m) of passing a predefined cross-section during the measurement period.

Density distribution (DD). the density of each cell is defined as the time (in percentage) it is occupied during the measurement period.

Travel time distribution (TTD). it is the distribution (described by the mean (μ_{MT}) and the standard deviation (σ_{MT})) of the time (in s) taken by a pedestrian to traverse the measurement area.

Average order parameter (AOP). it is a parameter quantifying lane formation, defined in (37) [22].

$$\Phi_{\mathrm{OP}} = \frac{1}{T_{\mathrm{OP}}} \sum\nolimits_{t=1}^{T_{\mathrm{OP}}} \varphi_{\mathrm{OP}}^{t} \tag{37}$$

With

$$\varphi_{\mathrm{OP}}^{t} = \frac{1}{N_{\mathrm{OP}}^{t}} \sum\nolimits_{n=1}^{N_{\mathrm{OP}}^{t}} \phi_{\mathrm{OP}}^{t,n} \tag{38}$$

$$\phi_{\mathrm{OP}}^{t,n} = \frac{\left(\phi_{\mathrm{OP,same}}^{t,n} - \phi_{\mathrm{OP,diff}}^{t,n}\right)^2}{\left(\phi_{\mathrm{OP,same}}^{t,n} + \phi_{\mathrm{OP,diff}}^{t,n}\right)^2} \in [0, 1] \tag{39}$$

where T_{OP} is the measurement duration (in s); $\varphi_{\mathrm{OP}}^{t}$ is an instantaneous order parameter reflecting how pronounced lanes are formed at t (the closer $\varphi_{\mathrm{OP}}^{t}$ is to 1, the more pronounced the self-organized lane formation is); N_{OP}^{t} is the number of pedestrians in the measurement area at t; $\phi_{\mathrm{OP,same}}^{t,n}$ is the number of pedestrians who have the same target exit as pedestrian n and move in n's lane at t, and $\phi_{\mathrm{OP,diff}}^{t,n}$ is the number of pedestrians who have a different target exit as pedestrian n and move in n's lane at t.

Note that the above metrics are only calculated at the defined measurement period [47]. This is to ensure that pedestrians experience the desired density level that is considered [47]. And, AOP is only determined in the bidirectional flow scenario. The normalized squared error related to the macroscopic and mesoscopic metrics is calculated by (40)-(41) respectively [46].

$$\mathrm{dist}_{\mathrm{M,ma}} = \frac{1}{N_{\mathrm{M}}^{2}} \sum\nolimits_{k=1}^{N_{\mathrm{M}}^{2}} \left(\frac{\sum_{q=1}^{N_{\mathrm{M}}^{1}} M_{\mathrm{sim}}^{k,q} / N_{\mathrm{M}}^{1} - M_{\mathrm{exp}}^{k}}{M_{\mathrm{norm}}^{k}} \right)^2 \tag{40}$$

$$\mathrm{dist}_{\mathrm{M,me}} = \frac{1}{2} \cdot \left(\frac{M_{\mathrm{sim},\mu} - M_{\mathrm{exp},\mu}}{M_{\mathrm{norm},\mu}} \right)^2 + \frac{1}{2} \cdot \left(\frac{M_{\mathrm{sim},\sigma} - M_{\mathrm{exp},\sigma}}{M_{\mathrm{norm},\sigma}} \right)^2 \tag{41}$$

where N_{M}^{2} is the number of travel directions in case of FR, the number of cells in case of DD, and 1 for AOP; N_{M}^{1} is the number of simulations; M_{sim} and M_{exp} respectively correspond to the simulated and observed values of the metric;M_{norm} is the value used for normalization [47].

Finally, the objective function is given by (42).

$$\mathrm{dist}_{\mathrm{M}} = \frac{3}{4} \cdot \left(\frac{1}{N_{\mathrm{M}}^{3} N_{\mathrm{M}}^{4}} \sum\nolimits_{i=1}^{N_{\mathrm{M}}^{3}} \sum\nolimits_{j=1}^{N_{\mathrm{M}}^{4}} \mathrm{dist}_{\mathrm{M}}^{i,j} \right) + \frac{1}{4} \cdot \mathrm{dist}_{\mathrm{M},\Phi_{\mathrm{op}}} \tag{42}$$

where N_{M}^{3} and N_{M}^{4} are, respectively, the number of scenarios and movement metrics; $\mathrm{dist}_{\mathrm{M}}^{i,j}$ is the normalized squared error between the simulated and observed values of movement metric j in scenario i; $\mathrm{dist}_{\mathrm{M},\Phi_{\mathrm{op}}}$ is the normalized squared error between simulated and observed values of Φ_{op}.

To make a fair comparison with the model of Fu et al. [6], the parameters of their model have to be first determined. The sensitivity parameter value of the dynamic field is set the same as that in our module (i.e., 0). As for the sensitivity parameter value of the static field, the aforementioned calibration procedures are applied to find the optimal value. Other parameters are determined by reproducing their work in one of the scenarios in [6] (for more details, the reader is referred to [33]). Due to the creation of jamming in setups M_2 and M_6 (bidirectional flow) given the chosen parameter setting (indicated by the prior simulations), Fu et al.'s model will not be tested and compared in bidirectional flow scenarios.

Moreover, sensitivity analyses are conducted to explore the impacts of the decision-making preferences on the locomotion efficiency of the pedestrian system by taking setups M_4, M_6 and M_8 as examples (one experiment for each movement scenario), see Tables II and IV. To this end, the whole evacuation process from the three setups is simulated, during which the **mean of individual evacuation times (MIET)** and the **flow rate (FR)** are measured. The evacuation from setup M_4 is regarded as the evacuation from a square room with one exit.

The main objective of these analyses is to determine whether the proposed locomotion movement module can reproduce the locomotion behaviour in real life (including locomotion movement and self-organized lane formation) and to evidence the performance advantages over the counterpart models, as well as to reveal how the decision-making preferences influence the system's locomotion efficiency.

3) The Integrated Framework: After the calibration and validation of each sub-module, to further evidence the validity of the whole framework in various scenarios, three real-life evacuations performed in different indoor environments are simulated. The average and the standard deviations of the **exit shares (ES)** and the **evacuation times (ET)** are measured in each simulation case.

The first case is the evacuation from a classroom with two exits [50], as shown in Fig. 5 (scene a). With the two exits half opened or completely opened, two evacuation experiments were conducted using 40 students. In this case, each cell occupies an area of 0.5 m $\times$ 0.5 m [50].

In the second case, the experiments performed by [51] are simulated. In their experiments, three groups composed of 10, 20 and 30 students were respectively instructed to complete 8, 8 and 16 evacuation experiments in a classroom with two exits, with varying student distributions in different experiments. The layout and the student distribution in one of the experiments are shown in Fig. 5 (scene b). According to [51], the size of each cell is 0.5 m $\times$ 0.5 m.

The third case concerns the evacuation from two rooms connected by up to three doors [52], as illustrated in Fig. 5 (scene c). To investigate the route choice behaviour, 46 students were instructed to pass through the experiment scenario as fast as possible when different doors are available, i.e., (1) only door 1 available, (2) doors 1 and 2 available, (3) doors 1 and 3 available, and (4) all doors available.

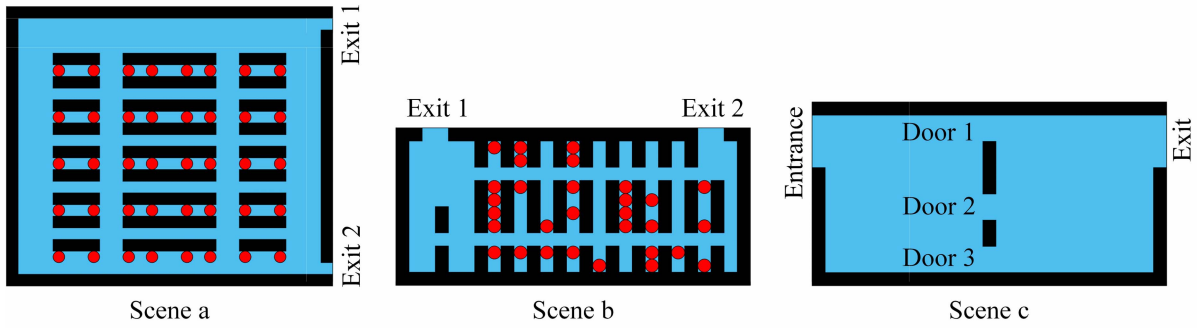

Fig. 5. Layout of the scenarios used for the simulations of the integrated framework. In scene a, exits 1 and 2 are half opened. The red circles represent the students standing in/sitting at the assigned positions.

TABLE V
A SUMMARY OF THE SIMULATION SETUPS

Module	Scenario	Comparison	Assessment metric
Exit choice and exit-choice changing	A square room with two or four exits [14]	Empirical data, and the module with EUT	ES, IEMP, ATCE, FCE, TET, MIET
Locomotion movement	Three movement scenarios [44]	Empirical data, the module with EUT, and the model of Fu, *et al.* [6]	FR, DD, TTD, AOP, TET, MIET
The overall framework	A classroom with two exits [50], a classroom with two exits [51], and two rooms connected by up to three doors [52]	Empirical data	ES, ET

TABLE VI
CALIBRATED PARAMETER VALUES FOR EXPERIMENT SETS 1 AND 2

Parameter	α_{E}	β_{E}	λ_{E}	γ_{E}	δ_{E}	$r_{d_{\mathrm{E}}}^{n}$	C_{R}	C_{A}
Set 1	1	0.56	1.92	0.8	0.8	0.68	0.4	0.2
Set 2	0.96	0.88	2.32	0.64	0.92	0.4	0.4	0.6

4) Summary: The simulation setups for the calibration and validation of three sub-modules and the overall model framework are summarized in Table V.

B. Results

This section presents the results of the case studies designed for each sub-module and the overall model framework to demonstrate the validity of the proposed algorithms in Section III.

1) Tactical-Level Decision Modules:

a) Calibration, validation and comparison: Table VI shows the set of parameter values with the best fitness for experiment sets 1 and 2. The results suggest that pedestrians are not risk-neutral and perfectly rational in making exit choice decisions. It can be seen that the main discrepancy between these two parameter sets lies in the value of β_{E}, λ_{E}, $r_{d_{\mathrm{E}}}^{n}$ and C_{A}. First, in setups T_6-T_8, the distribution of pedestrians is highly non-uniform, and thus the payoffs resulting from distance and crowdedness are contradictory. It is harder for pedestrians to make the optimal decision and thus irrationality and skew risk attitudes are more likely to occur. Accordingly, a much lower β_{E} (a higher degree of risk-seeking for losses) is observed in parameter set 1 than in set 2. This corresponds to a lower degree of loss aversion (a lower λ_{E}). It is also intuitively understandable that pedestrians in setups T_6-T_8 show a lower degree of stickiness to their original exit choice compared to those in other setups (i.e., a lower value of C_{A} in parameter set 1). Moreover, Liao et al. [14] and Luo et al. [53] found that the weight of "distance to exit" diminishes in pedestrians' tactical decision-making when the difference in the distances to the exits becomes smaller. Consistent with their findings [14], [53], the value of $r_{d_{\mathrm{E}}}^{n}$ in parameter set 2 is shown to be lower than set 1. The results imply that the tactical decision-making characteristics (e.g., preferences, weights of influential factors) vary, depending on the spatial environment of pedestrians.

The simulation errors related to the calibrated parameter values are listed in Table VII. It shows that the results from simulations are close to those from experiments except some cases related to metrics ATCE and FCE, which can also be

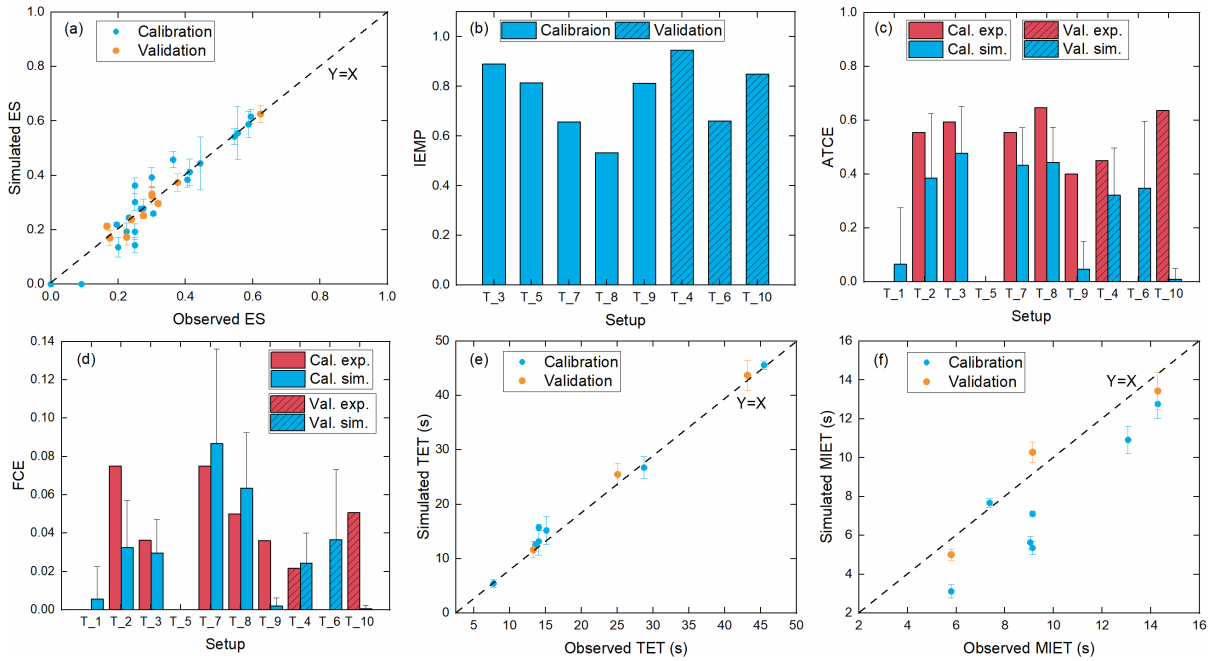

Fig. 6. Calibration and validation results of the tactical-level modules.

TABLE VII

THE SIMULATION ERRORS RELATED TO THE CALIBRATED PARAMETER SETS FOR THE TACTICAL-LEVEL DECISION MODULES

Error type	Set 1		Set 2				
	T_7	T_8	T_1	T_2	T_3	T_5	T_9
ES	0.245	0.112	0	0	0.015	0.140	0.023
IEMP	0.469	0.533	-	-	0.048	0.137	0.139
ATCE	0.479	1.322	0.137	0.514	0.425	0	3.976
FCE	0.646	0.843	0.146	0.649	0.202	0	5.505
TET	0.001	0	0.007	0.120	0	0.041	0.032
MIET	0.567	0.461	0.004	0.018	0.092	0.284	0.183
Weighted sum ($dist_E$)	0.502				0.428		

The acronyms identify the metrics (i.e., ES=exit share, IEMP=individual matching proportion, ATCE=average timing of changing the exit choice, FCE=frequency of changing the exit choice, TET=total evacuation time, MIET=mean of individual evacuation times)

seen in Fig. 6 (c) and (d). This could be ascribed to the scarce data related to the exit-choice changing behaviour due to its infrequency [14]. However, in both the calibration and validation, the coincidence degree between the simulated and observed results is high regarding metrics ES, IEMP, TET and MIET (shown in Fig. 6 (a), (b), (e) and (f)), which are the more common metrics used to represent the performance related to the tactical-level decisions in practical applications (e.g., behavioural optimization). The remaining discrepancies between the simulated and experimental results should be ascribed to factors other than distance and crowdedness that influence the tactical-level decisions, e.g., imitative behaviour [35], and individual heterogeneity [54].

Table VIII shows the prediction errors of the module with CPT and the module with EUT in simulating the exit choice behaviour. It can be seen that there are only three cases (denoted by the sign (*)) where the error of the module with CPT is slightly higher than that of the module with EUT. For quantitative comparisons, the relative error between these two modules is also computed in Table VIII. The results suggest that by-and-large, the module with CPT is superior to the module with EUT, with a 34.75% improvement in the prediction performance on average. This should be ascribed to the capability of CPT to delineate irrational decision-making preferences, and thus pedestrians' misinterpretations and human errors could be captured, leading to higher prediction accuracy. Moreover, greater prediction errors are found in setup T_6, compared with setups T_4 and T_10. As aforementioned, this should be ascribed to a higher degree of irrationality and skew risk attitudes of pedestrians in setups T_6-T_8, which makes it more difficult to predict the tactical-level decisions. Correspondingly, the module with CPT also has a

TABLE VIII
THE PREDICTION ERRORS RELATED TO THE MODULE WITH CPT AND THE MODULE WITH EUT

Setup	Model	ES	IEMP	TET	MIET
T_4	CPT	0	0.012	0.002	0.001
	EUT	0.006	0.014	0.009	0.015
	Ratio=(CPT-EUT)/EUT	**-1**	**-0.142**	**-0.778**	**-0.933**
T_6	CPT	0.035	0.460	0.022*	0.504
	EUT	1.253	0.683	0.016*	0.564
	Ratio=(CPT-EUT)/EUT	**-0.972**	**-0.327**	**0.375***	**-0.106**
T_10	CPT	0.026*	0.091*	0.002	0.139
	EUT	0.016*	0.081*	0.014	0.169
	Ratio=(CPT-EUT)/EUT	**0.625***	**0.123***	**-0.857**	**-0.178**

more prominent absolute error advantage in setup T_6 (e.g., 0.035 vs. 1.253).

b) Impacts of the decision-making preferences on exit choice: Fig. 7 shows the results of the sensitivity analyses related to metrics ES and IEMP. It can be seen that the direction of the effect of the decision-making preferences on the exit choice behaviour is similar in different setups, though the magnitude is varied. This suggests that our findings are by-and- large generic, independent of the evacuation setups.

In relation to the risk attitudes towards gains and losses (α_{E} and β_{E}), an opposite effect is observed (see Fig. 7 (a-1), (b-1) and (c-1)). And, an intermediate amount of deviation from 1 for α_{E} and β_{E} leads to the simulated exit choice behaviour closest to the observed one, too large or too small would make certain exits under-used or over-used. when $\alpha_{\mathrm{E}}/\beta_{\mathrm{E}}$ is lower than 1, pedestrians are risk aversive/risk seeking for gains/losses. It means that pedestrians prefer the exits with a sure gain to those with a substantial probability of a higher gain, while this is converse for losses, that is, the exits with a substantial probability of a larger loss are preferred over those with a sure loss. As $\alpha_{\mathrm{E}}/\beta_{\mathrm{E}}$ increases to exceed 1, the risk attitudes transition to risk-seeking/risk-aversion for gains/losses. And thus the responses of the exit choice behaviour to α_{E} and β_{E} are reverse each other. As for the degree of sensitivity to losses over gains (λ_{E}), the degree of match between the simulated and observed results generally increases with increasing λ_{E} (see Fig. 7 (a-2), (b-2) and (c-2)). In contrast, a high degree of distortion in probability judgment for losses and gains (i.e., low values of γ_{E} and δ_{E}) invariably exacerbates the discrepancy between the simulated and observed exit choice behaviour (see Fig. 7 (a-3), (b-3) and (c-3).

These results demonstrate the significant impact of the degree of rationality and risk attitudes on the exit choice behaviour at the macro (ES) and mesoscopic (IEMP) levels and thus suggest the importance of incorporating them in modelling exit choice decision-making.

TABLE IX
CALIBRATED PARAMETER VALUES

Parameter	α_{M}	β_{M}	λ_{M}	γ_{M}	δ_{M}	$r_{d_{\mathrm{M}}}^{n}$
Value	0.88	0.96	1.44	0.64	0.84	0.7

2) Locomotion movement module:

a) Calibration, validation and comparison: The parameter set implying irrationality and skew risk attitudes is found to have the optimal performance, see Table IX. In the model of Fu et al., the calibrated sensitivity parameter value of the static field is 1.7 (the original value is 2 or 0.8 in Fu et al. [6]). The simulation errors related to the calibrated parameter values of our and Fu et al.'s models are listed in Table X. It shows that the errors of all metrics except the DD are very small in both models, which justifies the calibration results. The relatively large error of the DD could be ascribed to the lack of details regarding the boundary conditions of the experiments, as indicated in [46].

Table XI shows the simulation performance of the module with CPT, the module with EUT and Fu et al.'s model in the six experiments of the three movement scenarios used for validation, which is assessed by the errors between the simulated and observed values of the four metrics. In the module with CPT, an error value close to zero is obtained for the FR in all setups, and the errors of the TTD and AOP are also rather low (less than 0.1) in setups M_6, M_7, M_8 and M_9. These results demonstrate the capability of the module with CPT to reproduce the locomotion movement in bottleneck flow, bidirectional flow and unidirectional corner flow scenarios. Moreover, it can be seen that the errors of the module with CPT are all smaller than that of the counterpart models except the four cases as follows. Specifically, compared with the module with CPT, the module with EUT performs better for the DD in M_6 and M_7 (denoted by the sign (*)) and Fu et al.'s model performs better for the FR and TTD in M_5 (denoted by the sign (**)). For quantitative comparisons, the relative error between our module and the counterpart models is also calculated and listed in Table XI. It is found that compared with the module with EUT and the model of Fu et al., the errors of the module with CPT are respectively reduced by 36.6% and 47.6% on average. Thus, in general, the results from the module with CPT are closer to those from experiments. This should be ascribed to the fact that our module includes a comprehensive decision-making process (compared with Fu et al.'s model) and are able to delineate irrational decision-making preferences (compared with the module using EUT).

To better investigate the capability of our module to reproduce the lane formation phenomenon, the time series of the instantaneous order parameter $\varphi_{\mathrm{OP}}^{t}$ during the measurement period in the three illustrative setups with different density levels (i.e., approximately 2.5, 2.0 and 0.7 per/m^2 in setups M_2, M_6 and M_7 respectively) in experiments and simulations using our module and Huang et al.'s model [33] are shown in Fig. 8 (a). The closer $\varphi_{\mathrm{OP}}^{t}$ is to 1, the more pronounced the lane formation phenomenon is. It can be found that in our module

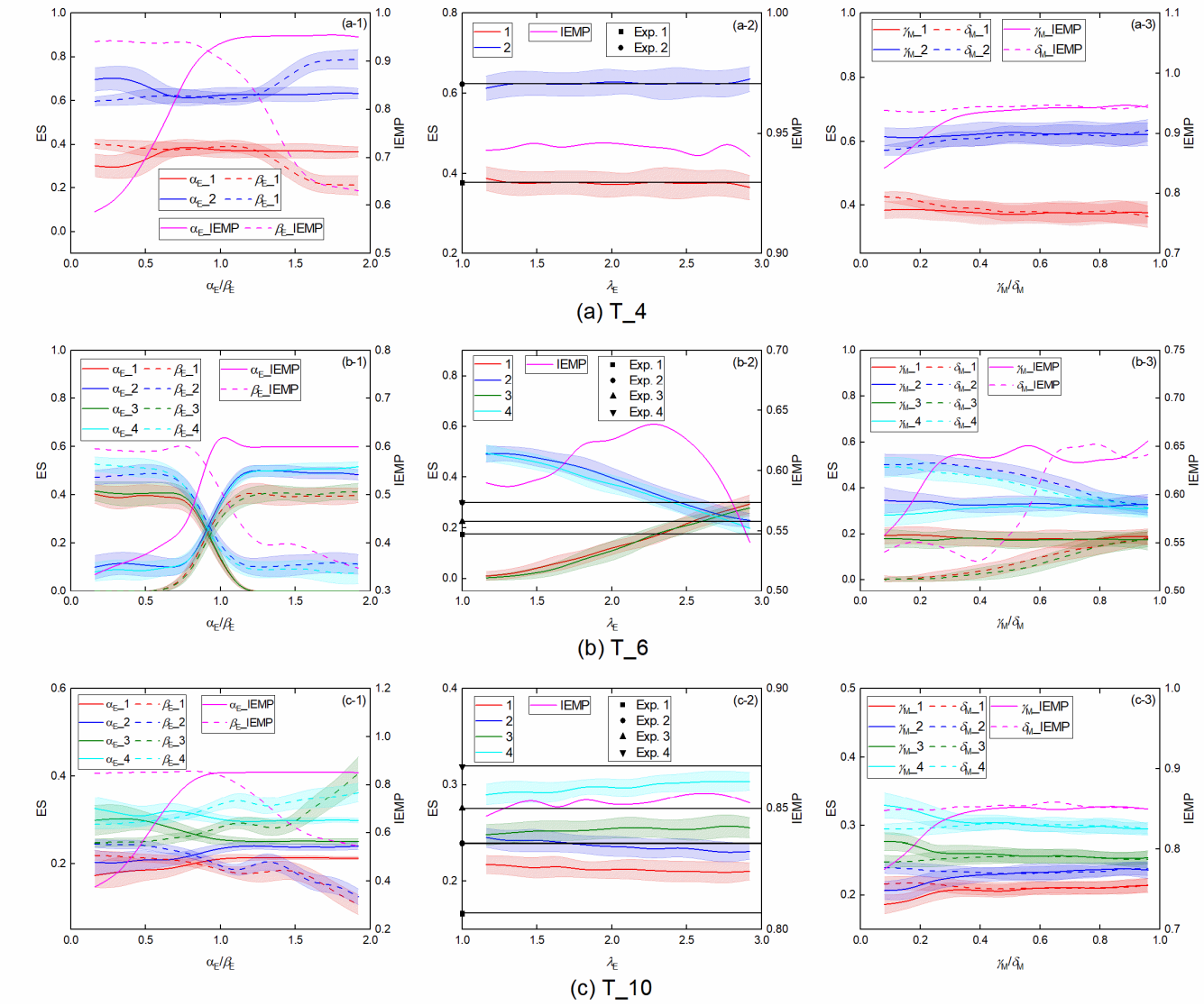

Fig. 7. The sensitivity of the exit shares (ES) and the individual-level exit choice matching proportion (IEMP) to the decision-making preferences in setups T_4, T_6 and T_10. In the plots, numbers '1', '2', '3', and '4' respectively represent the left, right, up, and bottom exits. The observed ES in each setup is also presented in the corresponding middle plot by the black lines.

TABLE X

CALIBRATION RESULTS OF THE LOCOMOTION MOVEMENT MODULE AND THE MODEL OF FU ET AL. [6]

Model	Setup	FR	DD	TTD	AOP	Weighted sum ($dist_M$)
CPT	M_1 (Bo)	0.044	0.397	0.190	-	0.171
	M_2 (Bi)	0.003	0.708	0.053	0.018	
	M_3 (Co)	0	0.564	0.040	-	
Fu et al.	M_1 (Bo)	0.134	0.565	0.004	-	0.570
	M_2 (Bi)	-	-	-	-	
	M_3 (Co)	0.089	2.115	0.514	-	

The acronyms identify the metrics (i.e., FR=Flow rate, DD=density distribution, TTD=travel time distribution, AOP=average order parameter) and the scenarios (i.e., Bi=bidirectional, Bo=Bottleneck, and Co=Corner)

though the simulated φ_{OP}^{t} is lower than that of the experiment at the beginning of the measurement period in some cases, it fast increases to a stable value after a certain period. According to the evaluation method defined in [49], under

TABLE XI

VALIDATION AND COMPARISON RESULTS OF THE MODULE WITH CPT, THE MODULE WITH EUT AND THE MODEL OF FU ET AL. BASED ON THE ERROR FROM THE FOUR METRICS

Setup	Model	FR	DD	TTD	AOP
M_4 (Bo)	CPT	0.011	0.388	0.269	-
	EUT	0.012	1.034	1.812	-
	Fu et al.	0.330	0.430	2.438	-
	Ratio=(CPT-EUT)/EUT	**-0.083**	**-0.625**	**-0.852**	-
	Ratio=(CPT-Fu)/Fu	**-0.967**	**-0.098**	**-0.890**	-
M_5 (Bo)	CPT	0.051**	1.01	0.211**	-
	EUT	0.041	1.839	4.789	-
	Fu et al.	0.034**	1.308	0.134**	-
	Ratio=(CPT-EUT)/EUT	**0.243**	**-0.451**	**-0.956**	-
	Ratio=(CPT-Fu)/Fu	**0.500****	**-0.228**	**0.575****	-
M_6 (Bi)	CPT	0	0.554*	0.021	0.044
	EUT	0	0.527*	0.046	0.230
	Ratio=(CPT-EUT)/EUT	**0**	**0.051***	**-0.543**	**-0.809**
M_7 (Bi)	CPT	0.002	0.144*	0.020	0.093
	EUT	0.002	0.114*	0.023	0.139
	Ratio=(CPT-EUT)/EUT	**0**	**0.263***	**-0.130**	**-0.331**
M_8 (Co)	CPT	0.003	0.374	0.038	-
	EUT	0.005	0.923	0.131	-
	Fu et al.	0.030	1.372	0.724	-
	Ratio=(CPT-EUT)/EUT	**-0.400**	**-0.595**	**-0.710**	-
	Ratio=(CPT-Fu)/Fu	**-0.900**	**-0.727**	**-0.948**	-
M_9 (Co)	CPT	0.001	0.505	0.005	-
	EUT	0.010	0.760	0.006	-
	Fu et al.	0.008	0.600	1.292	-
	Ratio=(CPT-EUT)/EUT	**-0.900**	**-0.336**	**-0.167**	-
	Ratio=(CPT-Fu)/Fu	**-0.875**	**-0.158**	**-0.996**	-

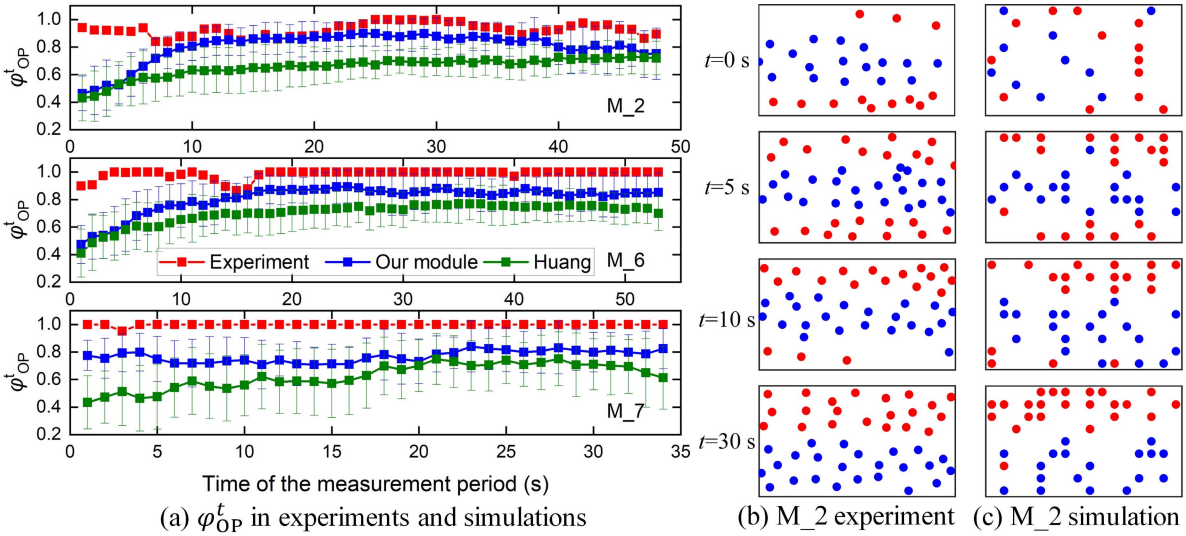

(a) φ_{OP}^{t} in experiments and simulations (b) M_2 experiment (c) M_2 simulation

Fig. 8. Results related to lane formation during the measurement period in experiments and simulations. Plot (a) shows the time series of φ_{OP}^{t} in setups M_2, M_6 and M_7 in experiments and simulations using our module and Huang et al.'s model [33]. Plots (b) and (c) respectively show the trajectory snapshots of setup M_2 in the experiment and simulation using our module, where the blue circles denote the pedestrians moving from the left to the right.

the density condition of 2.0 per/m^2, a stable state with the formation of lanes is developed much faster in our module than in Xu et al.'s model [49] (16.8 s vs. more than 75 s). It means that our module is able to rapidly lead to the formation of lanes. Moreover, in setups M_2, M_6 and M_7, the average φ_{OP}^{t} in the stable stage is respectively 0.85, 0.85 and 0.77 for our module, whereas this value is respectively 0.70, 0.73 and 0.66 in the same simulation conditions using Huang et al.'s

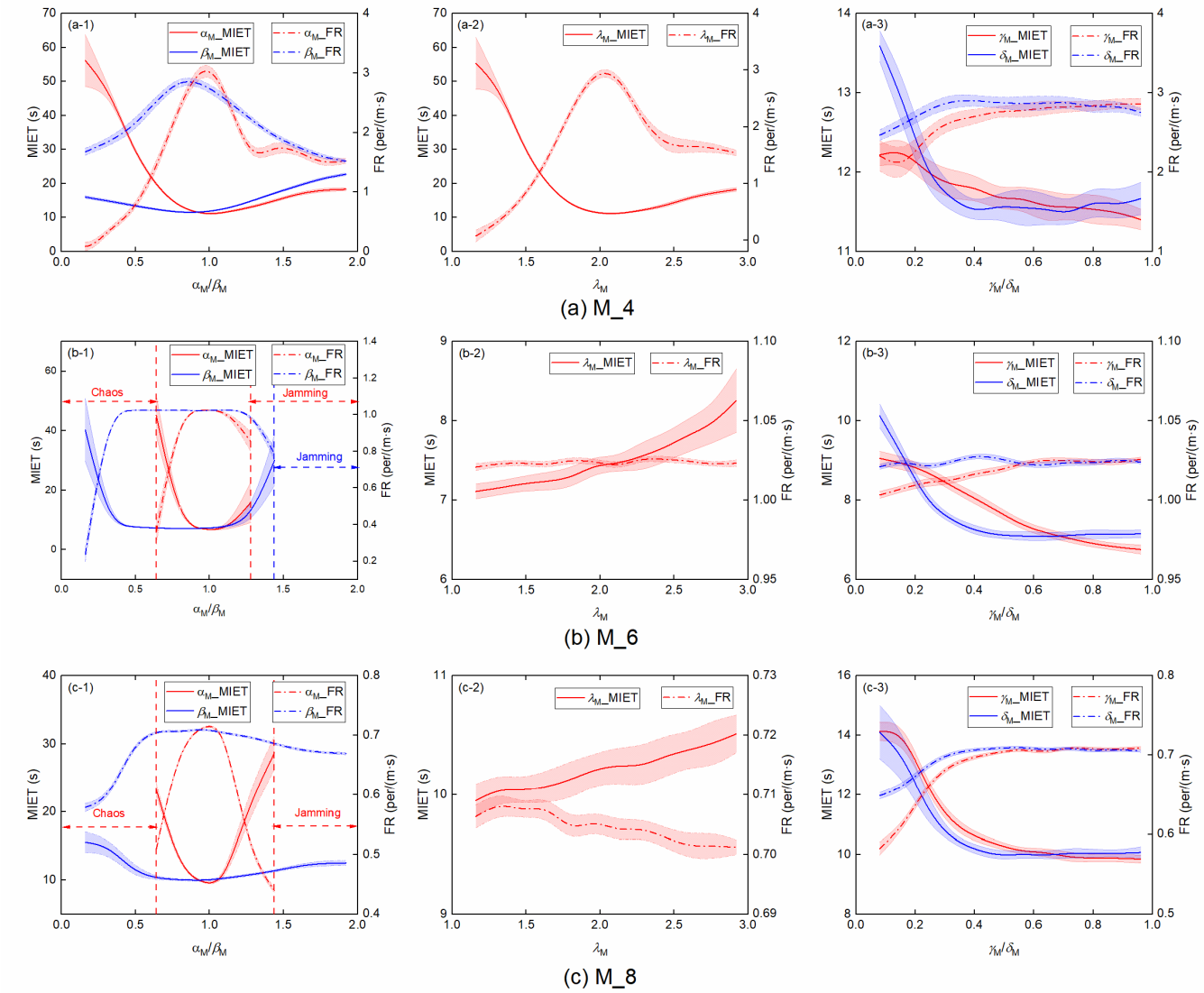

Fig. 9. Effects of the decision-making preferences on the mean of individual evacuation time (MIET) and the flow rate (FR) in setups M_4, M_6 and M_8.

model [33]. This indicates that our module performs much better than Huang et al.'s model [33] in reproducing lane formation (see Fig. 8 (a)). Taking setup M_2 as an example, the lane formation processes in the experiment and simulation using our module are visualized in Fig. 8 (b) and (c). It can be seen that in the simulation an ordered state with three lanes is first developed and then transitions to a two-lane state, which is similar to that observed in the experiment. These results demonstrate the capability of our module to reproduce lane formation in different density situations.

b) Impacts of the decision-making preferences on locomotion efficiency: According to the evacuation time and flow rate sensitivity analyses shown in Fig. 9, the sensitivity of the locomotion efficiency to the decision-making preference parameters is basically consistent in the three types of movement scenarios. This suggests the generalizability of our findings. In terms of the meso-level metric (the MIET) and the macro-level metric (the FR), the results suggest that the former measure to some degree can more acutely capture the variance of the system's locomotion efficiency (as shown in Fig. 9 (b-2) and (b-3)).

As for the impact of the parameters related to risk attitudes (α_M and β_M), a non-monotonic effect is observed. Zero deviation from 1 for α_M/β_M (i.e., risk-neutral) is not necessarily optimum for the system of pedestrians, and slightly skew risk attitudes could make the system more efficient (see Fig. 9 (a-1), (b-1) and (c-1)). When α_M/β_M is close to 0, pedestrians are significantly insensitive to the potential increase/decrease of gains/losses and thus preferred to the cells with a sure gain/a substantial probability of a larger loss, leading to a low locomotion efficiency or even a chaotic state featured with the unrealistic random movement (shown in Fig. 9 (b-1) and (c-1)). A moderate increment of α_M/β_M increases the sensitivity of pedestrians to the potential increase/decrease of gains/losses so that the cells with higher locomotion efficiency are identified and chosen. Nevertheless, a large value of α_M/β_M makes pedestrians become too radical for the opportunity to increase/decrease gains/losses to always

TABLE XII
SIMULATION (SIM) AND EXPERIMENT (EXP) RESULTS OF THE FIRST CASE

Results	Exit width	ES of exit 1	Maximum ET of exit 1 (s)	Maximum ET of exit 2 (s)	Average ET (s)
EXP	Half opened	0.45	9	8.5	5.4
SIM		**0.41±0.02**	**8.15±0.56**	**10.57±0.45**	**5.33±0.15**
EXP	Fully opened	0.45	7	6.5	4.2
SIM		**0.40±0.01**	**6.11±0.39**	**7.44±0.59**	**3.98±0.17**

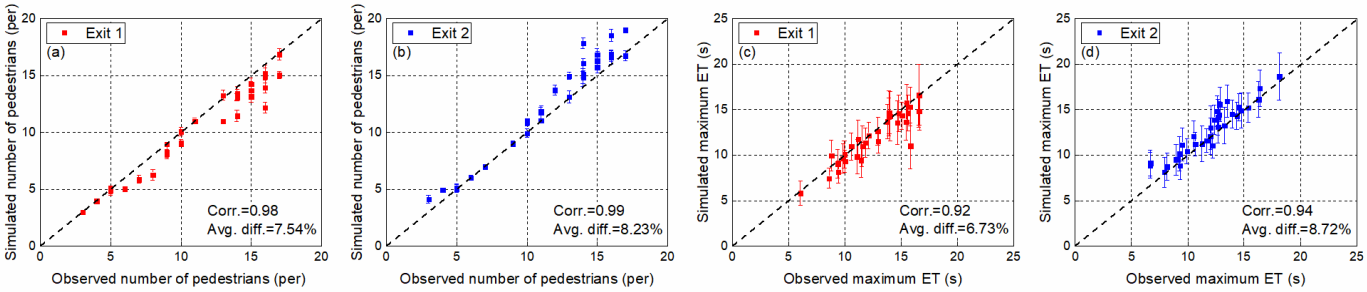

Fig. 10. The simulated and experimented results of the second case. Plots (a) and (b) show the comparison of the number of pedestrians evacuating from exits 1 and 2 between simulations and experiments. Plots (c) and (d) show the comparison of the maximum evacuation time (ET) of exits 1 and 2 between simulations and experiments. Also, the correlation (Corr.) and the average (absolute) difference (Avg. diff.) between simulated and experimented quantities are presented in each plot.

TABLE XIII
NUMBER OF PEDESTRIANS EVACUATING FROM THE THREE DOORS AND THE TOTAL EVACUATION TIME (ET) IN THE SIMULATIONS (SIM) AND EXPERIMENTS (EXP) FOR THE THIRD CASE

Results	Procedure	Door 1	Door 2	Door 3	Total ET (s)
EXP	1	46	0	0	24.31
SIM		**46**	**0**	**0**	**24.94±1.17**
EXP	2	23.25±1.26	22.75±1.26	0	19.42±0.37
SIM		**24.50±1.80**	**21.50±1.80**	**0**	**19.53±0.80**
EXP	3	28±1.41	0	18±41	19.55±0.27
SIM		**28.70±1.24**	**0**	**17.30±1.24**	**19.98±0.73**
EXP	4	20.75±1.89	18±1.41	7.25±3.03	19.06±0.49
SIM		**20.73±1.91**	**19.23±2.21**	**6.03±1.81**	**19.46±0.48**

choose the cells with a substantial probability of a higher gain/a sure loss at each time step. This conversely results in the under-used passageway and exit, and congestion or even jamming (shown in Fig. 9 (b-1) and (c-1)), which in turn reduces the system efficiency. This paradoxical effect is similar to the "faster-is-slower" phenomenon [3]. The results suggest that a slight degree of skew risk attitudes is not invariably detrimental to the system of pedestrians from the perspective of locomotion efficiency.

A higher value of λ_M indicates a greater degree of loss aversion. Though it plays a double-side role in the locomotion efficiency in setup M_4, an invariably negative effect is observed in setups M_6 and M_8, shown in Fig. 9 (a-2), (b-2) and (c-2). It means that its benefit to the evacuation system is scenario-dependent. However, high degrees of sensitivity to losses over gains (large values of λ_M) invariably harm the system regardless of the type of scenario.

In relation to γ_M and δ_M, large degrees of distortion in probability judgment invariably make the system inefficient (see Fig. 9 (a-3), (b-3) and (c-3)). $\gamma_M/\delta_M = 0$ represents a situation where the probability judgment is completely distorted, leading to the lowest locomotion efficiency. As the degree of distortion decreases, the system becomes more efficient. Such a promoting effect could vanish when γ_M/δ_M increases to exceed certain values. However, the results suggest that the system of pedestrians never benefits from any degree of distortion in probability judgment in locomotion decision-making.

These results suggest that the decision-making preferences of pedestrians play a significant role in the locomotion efficiency of the system, which could virtually benefit from certain irrational behaviours of pedestrians. The findings also highlight the importance to consider the decision-making preferences in modelling locomotion decision-making.

3) Validation of the integrated framework: The simulated and observed results of the three cases are respectively presented in Table XII, Fig. 10 and Table XIII, where in the tactical-level decision modules the calibrated parameter set 1 is used for the first two cases and set 2 for the third case. One can see that the results of our framework match well with

TABLE XIV
KEY NOTATION FOR THE THREE SUB-MODULES AND THE INTEGRATED FRAMEWORK

Key Notation	Description
Input	
$\mathbb{C}$	Environmental information of the geometry
ST^e	Set of the cells that can be traversed by pedestrians to evacuate through exit *e*
SF^e	Set of the static floor value of all cells to exit *e*
SD^e	Set of the distance of all cells to exit *e*
$D_{\mathrm{C}}^{e,(i,j)}$	Distance of cell (i,j) to exit *e*
$F_{\mathrm{C}}^{e,(i,j)}$	Static floor value of cell (i,j) to exit *e*
Exit choice module (Algorithm 1. EC-Determination)	
α_{E}, β_{E}, λ_{E}, γ_{E}, δ_{E}	Decision-making preference parameters of CPT in **EC-Determination**
$c_{\mathrm{E}}^{n,e}$	Crowdedness of pedestrian *n* to exit *e*
$d_{\mathrm{E}}^{n,e}$	Distance difference between the maximum distance to evacuate from $\mathbb{C}$ and the distance of pedestrian *n* to exit *e*
w_{E}^{e}	Width of exit *e*
$r_{\mathrm{E}}^{n,e}$	Movement resistance of pedestrian *n*'s shortest path to exit *e*
$\rho_{\mathrm{E}}^{e,1}$	Pedestrian density within a circular area with the midpoint of exit *e* as the center and a radius of $2w_{\mathrm{E}}^{e}$
$\rho_{\mathrm{E}}^{e,2}$	Pedestrian density between pedestrian *n* and exit *e*
m_{W}	Minimum width of all available exits in $\mathbb{C}$
m_{D}	Maximum distance to the exit in $\mathbb{C}$
$S_{\mathrm{E}}^{n,e}$	Set of the cells that constitute the shortest path of pedestrian *n* to exit *e*
$\rho^{e,(i,j)}$	Pedestrian density within the distance of three cells measured by Manhattan metric around cell $(i,j) \in S_{\mathrm{E}}^{ne}$
$N^{n,e,0}$	Number of pedestrians who target exit *e* and are closer to it than pedestrian *n* when exit *e* is chosen by pedestrian *n*
Exit-choice changing module (Algorithm 2. ECC-Determination)	
t	Cumulative time step of the evacuation
$t_{\mathrm{E}}^{n,e}$	Time step at which pedestrian *n* chooses exit *e*
$t_{\mathrm{BM}}^{n,e}$	Time step when pedestrian *n* begins moving towards exit *e*
N_{O}^{n}	Number of pedestrians within $\mathbb{C}$ when pedestrian *n* enters into it
$N_{\mathrm{EV}}^{n,t}$	Number of evacuated pedestrians from the time when pedestrian *n* enters into $\mathbb{C}$ to current time step *t*
N_{EC}^{n}	Number of changing the exit choice for pedestrian *n*
$N^{n,e,t}$	Number of pedestrians who target exit *e* and are closer to it than pedestrian *n* at *t*
$G_{\mathrm{R}}^{n,e,t}$	Relative crowdedness of target exit *e* for pedestrian *n* at *t*
$D_{\mathrm{P}}^{n,e,t}$	Distance of pedestrian *n* to target exit *e* at *t*
$M(SD^e)$	Maximum distance to target exit *e* in $\mathbb{C}$
C_{R}, C_{A}	Coefficient of the repulsive and attractive forces respectively
$R^{n,e,t}$, $A^{n,e,t}$	Repulsive and attractive forces of target exit *e* for pedestrian *n* at *t* respectively
$D_{\mathrm{L}}^{n,e,t}$	Pedestrian density of a semicircular visual zone (the depth of the view range is set to 2 m [57]) in front of pedestrian *n* when facing towards re-selected exit *e* at *t*.
Locomotion movement module (Algorithm 3. LM-Determination)	
α_{M}, β_{M}, λ_{M}, γ_{M}, δ_{M}	Decision-making preference parameters of CPT in **LM-Determination**
$\vec{D}^{k}$	Movement direction (*k*=1, 2, …, 8, represents eight directions that span anticlockwise from the east)
$\vec{D}_{\mathrm{C}}^{(i,j)}$, $\vec{D}_{\mathrm{A}}^{(i,j)}$	Calculated and actual desired directions of cell (i,j) respectively
ω^{n}	Pedestrian angular speed, set as π/s [58]
S_{L}	Length scale of discrete space
$\vec{D}^{n,t}$	Desired direction of pedestrian *n* at time step *t*
$P_{\mathrm{S}}^{n,t}$	Steering probability of pedestrian *n* at time step *t*
$x^{\vec{D}^{n,t}}$, $y^{\vec{D}^{n,t}}$	Horizontal and vertical axis coordinates of vector $\vec{D}^{n,t}$
$v^{n,t}$	Velocity of pedestrian *n* at *t*
$v_{\max}$	Maximum desired velocity of the system of pedestrians
v_{F}^{n}	Free velocity of pedestrian *n*
$SZ^{n,(i,j),k}$	Short-range visual zone bisected by $\vec{D}^{k}$ for pedestrian *n* located in cell (*i*, *j*), modelled as a cone, with an angle of $\pi/4$ and a length of L_{SZ}=2 m [57]
$\Omega_{\mathrm{SZ}}^{n,k}$	Set containing cells $(x_{\mathrm{SZ}}^{n,k}, y_{\mathrm{SZ}}^{n,k})$ within $SZ^{n,(i,j),k}$
$c_{\mathrm{M}}^{n,k,1}$	Cell-level movement resistance induced by the pedestrian density within $SZ^{n,(i,j),k}$
$c_{\mathrm{M}}^{n,k,2}$	Cell-level movement resistance induced by the potential collision within $SZ^{n,(i,j),k}$
$LZ^{n,(i,j),\ell}$ ($\ell \in \{\mathrm{L},\mathrm{M},\mathrm{R}\}$)	Long-range anticipation zone on the left (L), middle (M) and right (R) of pedestrian *n*, with a length of L_{LZ}=8 m
$\mathbb{Z}^{+}$	Set of positive integers
$\Omega_{\mathrm{LZ}}^{n,\ell}$	Set containing cells $(x_{\mathrm{LZ}}^{n,\ell}, y_{\mathrm{LZ}}^{n,\ell})$
λ_{LZ}	Long-range anticipation strength, set as 0.8 [22]
$c_{\mathrm{M}}^{n,k,3}$	Lane-level movement resistance induced by the potential collision within $LZ^{n,(i,j),\ell}$
$d_{\mathrm{M}}^{n,k}$, $c_{\mathrm{M}}^{n,k}$	Distance and crowdedness of moving towards $\vec{D}^{k}$ for pedestrian *n* respectively
The integrated framework (Algorithm 4. FFCA(N_{O}, $\mathbb{C}$))	
N_{O}	Number of pedestrians
N_{R}^{t}	Number of the remaining pedestrians at *t*.

those observed in experiments for the three cases, and thus its effectiveness and validity in reproducing real-life evacuations in different physical environments are further demonstrated. Moreover, it can be seen that in the first and second cases (see Table XII and Fig. 10 (a) and (b)), the number of pedestrians choosing exit 1 in simulations is slightly lower than that in experiments. This could be ascribed to the systematically different decision-making characteristics of pedestrians in the two cases and the experiments used for calibration. Furthermore, the simulation time of each run is respectively around 3.1 s, 2.6 s and 5.1 s for the three cases, which suggests that the proposed framework is capable of running faster than real-time and thus has great potential in practical applications [55] (e.g., real-time intelligent evacuation guiding systems).

V. Conclusion

This work is the pioneer to model the tactical and operational behaviours in evacuations with the perspective of decision-making under risk and uncertainty so that the significant but greatly overlooked decision-making preferences including bounded rationality and risk attitudes are encapsulated in microscopic pedestrian models. To this end, an innovative two-layer FFCA model framework consisting of three sub-modules is proposed. Based on the static navigation map constructed by the algorithm in [33], two behavioural modules with CPT respectively dedicated to modelling the exit choice and the locomotion behaviours are proposed. In the exit-choice changing module, attractive and repulsive forces are respectively quantified to delineate pedestrians' tendency of maintaining or changing the original choice. Moreover, for realistic behaviour modelling, various related decision-making factors are considered and computed by the proposed method, including distance, crowdedness and the desired direction. All sub-modules and the whole framework are validated in different indoor environments.

The calibrated parameter values of CPT (deviation from 1: non-perfect rationality) imply the existence of irrationality and skew risk attitudes in tactical and operational decision-making in real life. Performance comparisons evidence CPT's considerable superiority over EUT (the state-of-the-art approach) in the prediction accuracy of the exit choice and locomotion behaviours, with respectively 36.6% and 34.75% improvement on average. Also, the proposed locomotion movement module is able to reproduce self-organized lane formation in different density situations, and obtains the results closer to those from experiments, compared with Fu et al.'s model – the state-of-the-art CA model at the operational level (locomotion), with the errors reduced by 47.6% on average. Furthermore, simulation analyses suggest that the degree of rationality and risk attitudes have significant impacts on pedestrian tactical and operational decisions, and that certain irrational behaviours in decision-making could virtually benefit the evacuation system of pedestrians from the perspective of locomotion efficiency. These results highlight the necessity of revisiting decision-making in evacuations using an eligible theory (e.g., CPT) to refresh the existing knowledge, since UT which is commonly used in literature lacks the capability of capturing bounded rationality and risk attitudes in decision-making.

With the capability of reproducing tactical and operational decisions in real life, the proposed model framework can be used to predict pedestrian dynamics in indoor environments. And then, it is possible to optimize the evacuation performance not only from the traditional perspectives, i.e., architecture and route-planning, but also from decision-making preferences. This is particularly meaningful as it makes it possible to develop effective training and guidelines to help pedestrians establish appropriate decision-making preferences in daily life so that the potential misinterpretations and human errors can be reduced, and then they can make the optimal decisions in various environments under emergencies. This new perspective has significant practical implications for evacuation optimization and management.

Algorithm 1 EC-Determination(ST^e, SD^e, α_E, β_E, λ_E, γ_E, δ_E, $r^n_{d_E}$)

For all pedestrians n **do**
  For all exits e **do**
    Calculate $d^{n,e}_E$.
    Find pedestrian n's shortest path to exit e to generate $S^{n,e}_E$.
    For all cells $(i, j) \in S^{n,e}_E$ **do**
      Calculate $\rho^{e,(i,j)}$.
    End for
    Determine $\rho^{e,1}_E$, $\rho^{e,2}_E$ and $r^{n,e}_E$ to calculate $c^{n,e}_E$.
    Calculate exit e's prospect values induced by $d^{n,e}_E$ and $c^{n,e}_E$ based on CPT.
  End for
  Make the exit choice decision.
  Record $N^{n,e,0}$.
End for

Algorithm 2 ECC-Determination(ST^e, SD^e, $N^{n,e,0}$, N^n_O, $N^{n,t}_{EV}$, $t^{n,e}_{BM}$, N^n_{EC}, t, C_R, C_A)

For all pedestrians n **do**
  If $t^{n,e}_{BM} \neq 0 \& t > t^{n,e}_{BM}$ **then**
    Determine $c^{n,e}_E$, $N^{n,e,t}$, and $G^{n,e,t}_R$.
    Calculate $R^{n,e,t}$ and $A^{n,e,t}$.
    If $rand() < (R^{n,e,t} - A^{n,e,t})$ **then**
      Execute **EC-Determination**(ST^e, SD^e, α_E, β_E, λ_E, γ_E, δ_E, $r^n_{d_E}$) for pedestrian n to re-select an exit.
      If the target exit is changed **then**
        Calculate $D^{n,e,t}_L$.
        If $D^{n,e,t}_L < 3$ ped/m^2 **then**
          Change pedestrian n's target exit.
          $N^n_{EC} \leftarrow N^n_{EC} + 1$.
          Update $N^{n,e,0}$.
        End if
      End if
    End if
  End if
End for

Algorithm 3 LM-Determination(ST^e, SF^e, α_{M}, β_{M}, λ_{M}, γ_{M}, δ_{M}, $r^n_{d_{\mathrm{M}}}$, t)

For all pedestrians n located in cell (i, j) at time step t **do**
  Determine $\vec{D}^{(i,j)}_{\mathrm{A}}$.
  If $rand() < P^{n,t}_{\mathrm{S}}$ **then**
    $\vec{D}^{n,t} \leftarrow \vec{D}^{(i,j)}_{\mathrm{A}}$.
  End if
  Update $v^{n,t}$.
  If $rand() < v^{n,t}/v_{\max}$ **then**
    For all directions $\vec{D}^k$ with the neighbouring cell reachable by pedestrian n **do**
      Solve $\vec{\mathcal{V}}$ by equation constraints: $\vec{\mathcal{V}} \cdot \vec{D}^{n,t} = 0$ and $sign\left(\vec{\mathcal{V}} \times \vec{D}^{n,t}\right) - sign\left(\vec{D}^k \times \vec{D}^{n,t}\right) = 0$.
      Calculate $\left(x^{n,\ell}_{\mathrm{LZ}}, y^{n,\ell}_{\mathrm{LZ}}\right)$ to construct cell set $\Omega^{n,\ell}_{\mathrm{LZ}}$.
      Calculate $d^{n,k}_{\mathrm{M}}$ and $c^{n,k}_{\mathrm{M}}$.
      Calculate $\vec{D}^k$'s prospect values induced by $d^{n,k}_{\mathrm{M}}$ and $c^{n,k}_{\mathrm{M}}$ based on CPT.
      Determine the dynamic floor field value of the neighbouring cell of pedestrian n in $\vec{D}^k$.
    End for
    Make the locomotion decision considering the movement inertia towards $\vec{D}^{n,t}$
  If the target cell is occupied by other pedestrians **then**
    Pedestrian n stays still.
  End if
  End if
End for
Solve the conflicts between pedestrians.

Algorithm 4 FFCA($\mathbf{N_O}$, $\mathbb{C}$)

Execute the algorithm in [33] to create the static navigation map according to $\mathbb{C}$.
$t \leftarrow 1$, $N^t_{\mathrm{R}} \leftarrow N_{\mathrm{O}}$, and initialize the dynamic floor field.
While $N^t_{\mathrm{R}} > 0$ **do**
  For all pedestrians n entering into $\mathbb{C}$ at t **do**
    Execute **EC-Determination**(ST^e, SD^e, α_{E}, β_{E}, λ_{E}, γ_{E}, δ_{E}, $r^n_{d_{\mathrm{E}}}$) to determine pedestrians n's initial exit choice.
    Record N^n_{O}, $N^{n,t}_{\mathrm{EV}} \leftarrow 0$, $N^n_{\mathrm{EC}} \leftarrow 0$, and $t^{n,e}_{\mathrm{BM}} \leftarrow 0$.
  End for
  Execute **ECC-Determination**(ST^e, SD^e, $N^{n,e,0}$, N^n_{O}, $N^{n,t}_{\mathrm{EV}}$, $t^{n,e}_{\mathrm{BM}}$, N^n_{EC}, t, C_{R}, C_{A}) to determine whether pedestrian n changes the exit choice and if he/she does, which exit will be re-selected.
  Execute **LM-Determination**(ST^e, SF^e, α_{M}, β_{M}, λ_{M}, γ_{M}, δ_{M}, $r^n_{d_{\mathrm{M}}}$, t) to update pedestrians n's location.
  Update $N^{n,t}_{\mathrm{EV}}$ and $t^{n,e}_{\mathrm{BM}}$.
  $t \leftarrow t + 1$, $N^t_{\mathrm{R}} \leftarrow N^t_{\mathrm{R}} - 1$.
  Update the dynamic floor field for all cells according to the diffusion and decay rules in [5].
End while

In accordance with previous studies [14], [53], our calibration results show that the decision-making characteristics of pedestrians differ in different environments. Nonetheless, the validation results of the whole framework show the generalizability of the calibrated parameter sets. In practical applications, if the scenario of interest is similar to those used for calibration, these parameter sets can be directly used. Otherwise, a fine-tuning of the parameter sets according to the response laws revealed in the sensitivity analyses (in case of lacking eligible experimental data-sets) or a re-calibration task based on similar procedures (if eligible experimental data-sets are available) could be required.

In future work, this model framework could be improved in several aspects. First, it is warranted that dedicated empirical studies should be conducted to clarify pedestrians' mapping preference when estimating the evacuation outcomes based on the perceived uncertain information. Second, individual heterogeneity of decision-making preferences could be considered by collecting the decision-making empirical data at the individual level. Moreover, more accurate behaviour simulations could be achieved by a finer discretization of space and time, with the expense of computation efficiency. And also, this model framework can be extended to simulate evacuations from specific contexts (e.g., high-deck coaches [56]). To achieve this, the development of context-dependent behavioural rules may be needed.

APPENDIX

See Table XIV.

REFERENCES

[1] S. P. Hoogendoorn, F. L. M. van Wageningen-Kessels, W. Daamen, and D. C. Duives, "Continuum modelling of pedestrian flows: From microscopic principles to self-organised macroscopic phenomena," *Phys. A, Stat. Mech. Appl.*, vol. 416, pp. 684–694, Dec. 2014.

[2] D. C. Duives, W. Daamen, and S. P. Hoogendoorn, "State-of-the-art crowd motion simulation models," *Transp. Res. C, Emerg. Technol.*, vol. 37, pp. 193–209, Dec. 2013.

[3] D. Helbing, I. Farkas, and T. Vicsek, "Simulating dynamical features of escape panic," *Nature*, vol. 407, no. 6803, pp. 487–490, 2000.

[4] S. Liu, S. Lo, J. Ma, and W. Wang, "An agent-based microscopic pedestrian flow simulation model for pedestrian traffic problems," *IEEE Trans. Intell. Transp. Syst.*, vol. 15, no. 3, pp. 992–1001, Jun. 2014.

[5] C. Burstedde, K. Klauck, A. Schadschneider, and J. Zittartz, "Simulation of pedestrian dynamics using a two-dimensional cellular automaton," *Phys. A, Stat. Mech. Appl.*, vol. 295, pp. 507–525, Jun. 2001.

[6] Z. Fu, Q. Jia, J. Chen, J. Ma, K. Han, and L. Luo, "A fine discrete field cellular automaton for pedestrian dynamics integrating pedestrian heterogeneity, anisotropy, and time-dependent characteristics," *Transp. Res. C, Emerg. Technol.*, vol. 91, pp. 37–61, Jun. 2018.

[7] S. P. Hoogendoorn and P. H. Bovy, "Pedestrian route-choice and activity scheduling theory and models," *Transp. Res. B, Methodol.*, vol. 38, no. 2, pp. 169–190, 2004.

[8] R. Huang, X. Zhao, Y. Yuan, Q. Yu, C. Zhou, and W. Daamen, "Experimental study on evacuation behaviour of passengers in a high-deck coach: A Chinese case study," *Phys. A, Stat. Mech. Appl.*, vol. 579, Oct. 2021, Art. no. 126120.

[9] H. Dong, M. Zhou, Q. Wang, X. Yang, and F.-Y. Wang, "State-of-the-art pedestrian and evacuation dynamics," *IEEE Trans. Intell. Transp. Syst.*, vol. 21, no. 5, pp. 1849–1866, May 2019.

[10] J. Von Neumann and O. Morgenstern, *Theory of Games and Economic Behavior*. Princeton, NJ, USA: Princeton Univ. Press, 1944.

[11] D. C. Duives and H. S. Mahmassani, "Exit choice decisions during pedestrian evacuations of buildings," *Transp. Res. Rec., J. Transp. Res. Board*, vol. 2316, no. 1, pp. 84–94, Jan. 2012.

[12] R. Lovreglio, D. Borri, L. dell'Olio, and A. Ibeas, "A discrete choice model based on random utilities for exit choice in emergency evacuations," *Saf. Sci.*, vol. 62, pp. 418–426, Feb. 2014.

[13] B. L. Mesmer and C. L. Bloebaum, "Modeling decision and game theory based pedestrian velocity vector decisions with interacting individuals," *Saf. Sci.*, vol. 87, pp. 116–130, Aug. 2016.

[14] W. Liao, A. U. Kemloh Wagoum, and N. W. F. Bode, "Route choice in pedestrians: Determinants for initial choices and revising decisions," *J. Roy. Soc. Interface*, vol. 14, no. 127, Feb. 2017, Art. no. 20160684.

[15] M. Haghani and M. Sarvi, "Stated and revealed exit choices of pedestrian crowd evacuees," *Transp. Res. B, Methodol.*, vol. 95, pp. 238–259, Jan. 2017.

[16] S. Cao, L. Fu, and W. Song, "Exit selection and pedestrian movement in a room with two exits under fire emergency," *Appl. Math. Comput.*, vol. 332, pp. 136–147, Sep. 2018.

[17] B. Yu, "Consideration of tactical decisions in microscopic pedestrian simulation: Algorithm and experiments," *Transp. Res. C, Emerg. Technol.*, vol. 119, Oct. 2020, Art. no. 102742.

[18] X. Wang, C. Mohcine, J. Chen, R. Li, and J. Ma, "Modeling boundedly rational route choice in crowd evacuation processes," *Saf. Sci.*, vol. 147, Mar. 2022, Art. no. 105590.

[19] T. Kretz, "Pedestrian traffic: On the quickest path," *J. Stat. Mech., Theory Exp.*, vol. 2009, no. 3, Mar. 2009, Art. no. P03012.

[20] R.-Y. Guo, H.-J. Huang, and S. C. Wong, "Route choice in pedestrian evacuation under conditions of good and zero visibility: Experimental and simulation results," *Transp. Res. B, Methodol.*, vol. 46, no. 6, pp. 669–686, Jul. 2012.

[21] Y. Suma, D. Yanagisawa, and K. Nishinari, "Anticipation effect in pedestrian dynamics: Modeling and experiments," *Phys. A, Stat. Mech. Appl.*, vol. 391, nos. 1–2, pp. 248–263, Jan. 2012.

[22] S. Nowak and A. Schadschneider, "Quantitative analysis of pedestrian counterflow in a cellular automaton model," *Phys. Rev. E, Stat. Phys. Plasmas Fluids Relat. Interdiscip. Top.*, vol. 85, no. 6, Jun. 2012, Art. no. 066128.

[23] D. L. Gao, E. W. Ming Lee, and Y. Y. Lee, "Integration of cumulative prospect theory in cellular automata model for building evacuation," *Int. J. Disaster Risk Reduction*, vol. 74, May 2022, Art. no. 102904.

[24] I. N. Durbach and T. J. Stewart, "Modeling uncertainty in multi-criteria decision analysis," *Eur. J. Oper. Res.*, vol. 223, no. 1, pp. 1–14, Nov. 2012.

[25] D. Kahneman and A. Tversky, "Prospect theory: An analysis of decision under risk," *Econometrica*, vol. 47, no. 2, pp. 363–391, 1979.

[26] A. Tversky and D. Kahneman, "Advances in prospect theory: Cumulative representation of uncertainty," *J. Risk Uncertainty*, vol. 5, no. 4, pp. 297–323, 1992.

[27] G. de Moraes Ramos, W. Daamen, and S. Hoogendoorn, "Modelling travellers' heterogeneous route choice behaviour as prospect maximizers," *J. Choice Model.*, vol. 6, pp. 17–33, Mar. 2013.

[28] J. Yang and G. Jiang, "Development of an enhanced route choice model based on cumulative prospect theory," *Transp. Res. C, Emerg. Technol.*, vol. 47, pp. 168–178, Oct. 2014.

[29] S. Gao, E. Frejinger, and M. Ben-Akiva, "Adaptive route choices in risky traffic networks: A prospect theory approach," *Transp. Res. C, Emerg. Technol.*, vol. 18, no. 5, pp. 727–740, Oct. 2010.

[30] M. Haghani and M. Sarvi, "'Rationality' in collective escape behaviour: Identifying reference points of measurement at micro and macro levels," *J. Adv. Transp.*, vol. 2019, Aug. 2019, Art. no. 2380348.

[31] D. L. Gao, W. Xie, and E. W. Ming Lee, "Individual-level exit choice behaviour under uncertain risk," *Phys. A, Stat. Mech. Appl.*, vol. 604, Oct. 2022, Art. no. 127873.

[32] J. B. Yang, "Rule and utility based evidential reasoning approach for multiattribute decision analysis under uncertainties," *Eur. J. Oper. Res.*, vol. 131, no. 1, pp. 31–61, 2001.

[33] R. Huang, X. Zhao, C. Zhou, L. Kong, C. Liu, and Q. Yu, "Static floor field construction and fine discrete cellular automaton model: Algorithms, simulations and insights," *Phys. A, Stat. Mech. Appl.*, vol. 606, Nov. 2022, Art. no. 128150.

[34] S. Chen, H. Fu, Y. Qiao, and N. Wu, "Route choice behavior modeling for emergency evacuation and efficiency analysis based on type—II fuzzy theory," *IEEE Trans. Intell. Transp. Syst.*, vol. 23, no. 7, pp. 6934–6949, Jul. 2022.

[35] M. Haghani and M. Sarvi, "Simulating dynamics of adaptive exit-choice changing in crowd evacuations: Model implementation and behavioural interpretations," *Transp. Res. C, Emerg. Technol.*, vol. 103, pp. 56–82, Jan. 2019.

[36] D. Yanagisawa et al., "Introduction of frictional and turning function for pedestrian outflow with an obstacle," *Phys. Rev. E, Stat. Phys. Plasmas Fluids Relat. Interdiscip. Top.*, vol. 80, no. 3, Sep. 2009, Art. no. 036110.

[37] U. Weidmann, "Transporttechnik der fußgänger: Transporttechnische eigenschaften des fußgängerverkehrs, literaturauswertung," in *IVT Schriftenreihe*, vol. 90. Zürich, Switzerland: ETH Zürich, Institut für Verkehrsplanung, Transporttechnik, Strassen- und Eisenbahnbau (IVT), 1993.

[38] A. Kirchner and A. Schadschneider, "Simulation of evacuation processes using a bionics-inspired cellular automaton model for pedestrian dynamics," *Phys. A, Stat. Mech. Appl.*, vol. 312, pp. 260–276, Sep. 2002.

[39] S. Ghader, A. Darzi, and L. Zhang, "Modeling effects of travel time reliability on mode choice using cumulative prospect theory," *Transp. Res. C, Emerg. Technol.*, vol. 108, pp. 245–254, Nov. 2019.

[40] Q. Yan, T. Feng, and H. Timmermans, "Investigating private parking space owners' propensity to engage in shared parking schemes under conditions of uncertainty using a hybrid random-parameter logit-cumulative prospect theoretic model," *Transp. Res. C, Emerg. Technol.*, vol. 120, Nov. 2020, Art. no. 102776.

[41] E. Ronchi, P. A. Reneke, and R. D. Peacock, "A method for the analysis of behavioural uncertainty in evacuation modelling," *Fire Technol.*, vol. 50, no. 6, pp. 1545–1571, Nov. 2014.

[42] N. Guo, Q.-Y. Hao, R. Jiang, M.-B. Hu, and B. Jia, "Uni- and bi-directional pedestrian flow in the view-limited condition: Experiments and modeling," *Transp. Res. C, Emerg. Technol.*, vol. 71, pp. 63–85, Oct. 2016.

[43] M. M. Wright, *Lecture Notes on the Mathematics of Acoustics*. Singapore: World Scientific, 2004.

[44] C. Keip and K. Ries, "Dokumentation von versuchen zur personenstrom-dynamik," Project Hermes, Bergische Universität Wuppertal, Tech. Rep., 2009.

[45] W. Daamen, C. Buisson, and S. P. Hoogendoorn, *Traffic Simulation and Data: Validation Methods and Applications*. Boca Raton, FL, USA: CRC Press, 2014.

[46] M. Sparnaaij, D. C. Duives, V. L. Knoop, and S. P. Hoogendoorn, "Multiobjective calibration framework for pedestrian simulation models: A study on the effect of movement base cases, metrics, and density levels," *J. Adv. Transp.*, vol. 2019, pp. 1–18, Jul. 2019.

[47] M. Sparnaaij, "How to calibrate a pedestrian simulation model: An investigation into how the choices of scenarios and metrics influence the calibration," M.S. thesis, Dept. Transp. Planning, Delft Univ. Technol., Delft, The Netherlands, 2017.

[48] D. C. Duives, "Analysis and modelling of pedestrian movement dynamics at large-scale events," Ph.D. dissertation, Dept. Transp. Planning, Delft Univ. Technol., Delft, The Netherlands, 2016.

[49] Q. Xu, M. Chraibi, and A. Seyfried, "Anticipation in a velocity-based model for pedestrian dynamics," *Transp. Res. C, Emerg. Technol.*, vol. 133, Dec. 2021, Art. no. 103464.

[50] S. Liu, L. Yang, T. Fang, and J. Li, "Evacuation from a classroom considering the occupant density around exits," *Phys. A, Stat. Mech. Appl.*, vol. 388, no. 9, pp. 1921–1928, May 2009.

[51] R.-Y. Guo, H.-J. Huang, and S. C. Wong, "A potential field approach to the modeling of route choice in pedestrian evacuation," *J. Stat. Mech., Theory Exp.*, vol. 2013, no. 2, Feb. 2013, Art. no. P02010.

[52] L. Crociani, G. Vizzari, D. Yanagisawa, K. Nishinari, and S. Bandini, "Route choice in pedestrian simulation: Design and evaluation of a model based on empirical observations," *Intelligenza Artificiale*, vol. 10, no. 2, pp. 163–182, Jan. 2016.

[53] L. Luo, B. Zhang, B. Guo, J. Zhong, and W. Cai, "Why they escape: Mining prioritized fuzzy decision rule in crowd evacuation," *IEEE Trans. Intell. Transp. Syst.*, vol. 23, no. 10, pp. 19456–19470, Oct. 2022.

[54] Y. Hu, J. Zhang, W. Song, and N. W. F. Bode, "Social groups barely change the speed-density relationship in unidirectional pedestrian flow, but affect operational behaviours," *Saf. Sci.*, vol. 139, Jul. 2021, Art. no. 105259.

[55] Y. Liu, S. Ke, Z. Fang, M. H. Cheung, W. Cai, and J. Huang, "A storage sustainability mechanism with heterogeneous miners in blockchain," *IEEE J. Sel. Areas Commun.*, vol. 40, no. 12, pp. 3645–3659, Dec. 2022.

[56] R. Huang, X. Zhao, Y. Yuan, Q. Yu, and W. Daamen, "Open experimental data-sets to reveal behavioural insights of high-deck coach evacuations," *Fire Technol.*, vol. 58, pp. 2313–2356, May 2022.

[57] R. Zhao, Y. Zhai, L. Qu, R. Wang, Y. Huang, and Q. Dong, "A continuous floor field cellular automata model with interaction area for crowd evacuation," *Phys. A, Stat. Mech. Appl.*, vol. 575, Aug. 2021, Art. no. 126049.

[58] Z. Fu, Q. Deng, A. Schadschneider, Y. Li, and L. Luo, "Resolution of deadlocks in a fine discrete floor field cellular automata model—Modeling of turning and lateral movement at bottlenecks," *J. Stat. Mech., Theory Exp.*, vol. 2019, no. 12, Dec. 2019, Art. no. 123402.

Rong Huang received the B.Sc. degree in vehicle engineering from Chang'an University, Xi'an, China, in 2017, where he is currently pursuing the Ph.D. degree.

Since October 2021, he has been working as a Visiting Ph.D. Student with the Department of Transport and Planning, Delft University of Technology. His research interests include passenger and pedestrian dynamics, evacuation modeling, and simulation.

Xuan Zhao received the B.Sc., M.Sc., and Ph.D. degrees in vehicle engineering from Chang'an University, Xi'an, China, in 2007, 2009, and 2012, respectively. He is currently a Professor with the School of Automobile, Chang'an University. He has undertaken over ten government sponsored works, including the National Key Research and Development Program of China, the National Natural Science Foundation of China, and the China Post-Doctoral Science Foundation. His research interests include pedestrian dynamics, fire safety, vehicle control strategy, and safety design theory.

Yufei Yuan received the M.Sc. degree in transport and planning and the Ph.D. degree from the Delft University of Technology (TU Delft), Delft, The Netherlands, in 2008 and 2013, respectively. He is currently a Tenured Researcher with the Department of Transport and Planning, TU Delft. His research interests include traffic flow theory and simulation, data mining and processing, traffic state estimation and prediction, traffic management and analysis under evacuations, and intelligent transportation systems in general for "fast" vehicular traffic. Until recently, his working area is extending to "slow/active modes," including pedestrian and bicyclist flows and covering from modeling underpinning to simulation implementation.

Qiang Yu received the B.Sc., M.Sc., and Ph.D. degrees in vehicle engineering from Chang'an University, Xi'an, China, in 1982, 1985, and 2000, respectively. He is currently a Professor with the School of Automobile, Chang'an University. He has authored four books and undertaken over 20 government sponsored works. His research interests include vehicle dynamics and safety design, and passenger safety.

Chengqing Liu received the B.Sc. and M.Sc. degrees in logistics engineering, transportation engineering from Chang'an University, Xi'an, China, in 2017 and 2020, respectively. She is currently a System Optimization and Management Engineer at CISDI Engineering Company Ltd., CISDI Group Company Ltd., Chongqing, China. Her research interests include routing planning and algorithm optimization.

Winnie Daamen received the Ph.D. degree in transport and planning from the Delft University of Technology (TU Delft), Delft, The Netherlands, in 2004.

She is currently an Associate Professor with the Department of Transport and Planning, TU Delft. Her research interests include data collection (offline and real-time, for all modes) and analyses, theory and model formulation, model implementation, and management for pedestrians and cyclists.

Dr. Daamen is a member of the Pedestrian and Evacuation Dynamics (PED) and Traffic and Granular Flow (TGF) Steering Committee. She is also an Associate Editor of the IEEE OPEN JOURNAL OF THE INTELLIGENT TRANSPORTATION SYSTEMS SOCIETY and a member of the Editorial Advisory Board of *Transportation Research Part C: Emerging Technologies* and *Physica A: Statistical Mechanics and its Applications*.